

UNCLASSIFIED

AD NUMBER

AD006996

CLASSIFICATION CHANGES

TO: unclassified

FROM: confidential

LIMITATION CHANGES

TO:
Approved for public release; distribution is unlimited.

FROM:
Distribution authorized to DoD only; Administrative/Operational Use; FEB 1953. Other requests shall be referred to David Taylor Model Basin, Washington, DC. Pre-dates formal DoD distribution statements. Treat as DoD only.

AUTHORITY

28 Feb 1965 per DoDD 5200.10; David W Taylor Naval Ship R&D Ctr ltr dtd 7 Oct 1980

THIS PAGE IS UNCLASSIFIED

UNCLASSIFIED

AD _____

DEFENSE DOCUMENTATION CENTER

FOR

SCIENTIFIC AND TECHNICAL INFORMATION

CAMERON STATION ALEXANDRIA, VIRGINIA

DOWNGRADED AT 3 YEAR INTERVALS:
DECLASSIFIED AFTER 12 YEARS
DCD DIR 5200.10



UNCLASSIFIED

THIS REPORT HAS BEEN DECLASSIFIED
AND CLEARED FOR PUBLIC RELEASE.

DISTRIBUTION A
APPROVED FOR PUBLIC RELEASE;
DISTRIBUTION UNLIMITED.

AD No. 6996

ASTIA FILE COPY

**NAVY DEPARTMENT
THE DAVID W. TAYLOR MODEL BASIN
WASHINGTON 7, D.C.**

**RESPONSE OF STIFFENED CYLINDRICAL SHELLS
TO COMBINED HYDROSTATIC LOADING
AND STEADY-STATE LOBAR VIBRATIONS.
PART I - TESTS OF MODELS DR201 AND DR202
DESIGNED TO FAIL BY SHELL YIELD**

by
Ralph B. Allnutt



SECURITY INFORMATION

RESPONSE OF STIFFENED CYLINDRICAL SHELLS TO COMBINED HYDROSTATIC LOADING AND STEADY-STATE LOBAR VIBRATIONS

PART 1 - TESTS OF MODELS DR201 AND DR202 DESIGNED TO FAIL BY SHELL YIELD

by

Ralph B. Allnutt

"This document contains information affecting the national defense of the United States within the meaning of the Espionage Laws, Title 18, U.S. C., Sections 793 and 794. The transmission or the revelation of its contents in any manner to an unauthorized person is prohibited by law."

"Reproduction of this document in any form by other than naval activities is not authorized except by special approval of the Secretary of the Navy or the Chief of Naval Operations as appropriate."

February 1953

(Report C-445)
NS 724-012
NS 731-038

SECURITY INFORMATION

TABLE OF CONTENTS

	Page
ABSTRACT	1
INTRODUCTION	1
DESCRIPTION OF MODELS	3
INSTRUMENTATION AND TEST PROCEDURES	5
RESULTS	9
DISCUSSION OF RESULTS	20
COMPARISON OF OBSERVED AND COMPUTED RESONANCE FREQUENCIES	25
CONCLUSIONS	30
APPENDIX	32
REFERENCES	36

ABSTRACT

Several exploratory tests have been conducted with stiffened circular cylinders to determine the possible weakening in hydrostatic strength produced by steady-state lobar vibrations. This mode of response involves deformations of the frame-and-shell combination in transverse planes such that longitudinal corrugations occur which vary sinusoidally in amplitude between holding bulkheads. This report describes the results of tests on an identical pair of models designed to fail under hydrostatic pressure by yielding of the shell.

In these tests, one model was subjected to hydrostatic pressure alone while the other was subjected to combined hydrostatic pressure and steady-state radial vibration. As a result the vibrated model failed at a lower hydrostatic pressure; each model exhibited the same mode of failure (shell yield). The observed reduction in collapse pressure was attributed to superposition of vibratory stresses on static stresses.

The investigation also included:

1. Correlation of the measured natural frequencies with those theoretically possible based on analysis of the stiffened shell as a collection of elastically supported rings and on Bleich's analysis of the combined action of frame, shell, and bulkhead.
2. Study of effects of hydrostatic pressure on the amplitude of response at resonance with a constant driving force.
3. Determination of virtual mass of surrounding water at resonance frequencies.
4. Study of effects of hydrostatic pressure on the resonance frequencies.

INTRODUCTION

To further the understanding of the mechanism of failure of submarines under enemy attack at great depth, it was desired to determine the contribution of the lobar mode of response to collapse of submarine pressure hulls subjected to underwater explosions. The possible importance of this mode of dynamic response has been under serious consideration in submarine research only during the past several years, mainly as a result of work initiated at the David Taylor Model Basin in the latter part of 1949.¹⁻³

Although not conclusively demonstrated, it is considered that with a submarine some portion of the response to explosive attack occurs in a lobar mode, that is, the frame-and-shell

¹References are listed on page 36.

combination deforms in transverse planes such that longitudinal corrugations occur which vary more or less sinusoidally in amplitude between holding bulkheads. Actually, many such modes may be developed simultaneously with various phase relationships and amplitudes which depend on the characteristics of the structure and of the loading. The study of this response under actual explosive conditions is complicated by the variety of modes excited and the lack of control over variations in the loading pulse. Thus, as a means of developing some fundamental data regarding the effect of lobar response on strength, these exploratory tests were conducted using steady-state excitation such that response in any selected mode could be readily determined under controlled conditions. In order that the damaging effects of such vibration might be evaluated, the tests were conducted with combined pressure and vibratory loading to investigate specifically the possible weakening in hydrostatic strength which would be engendered by the vibrations, excited either by a vibrator or by transient loading.

In addition to its possible influence on hull strength this mode of dynamic response may warrant further consideration in other research studies pertaining to underwater noise generated by submarines and to the effectiveness of shock mounts.

Although these tests were necessarily of an exploratory nature, since no record of similar work exists, as many definite objectives were set as were deemed practicable. Specifically, the objectives of the tests were:

1. To determine whether the collapse pressure of a submarine pressure hull is adversely affected by the superposition of lobar vibration upon hydrostatic pressure.
2. To determine whether the mode of collapse is altered by the above combined action.
3. To obtain additional information to supplement present knowledge of the dynamic characteristics of stiffened cylindrical shells when subjected to radial excitation and to correlate the measured natural frequencies with those theoretically possible on the basis of analyses of the stiffened shell as a collection of elastically supported rings.
4. To determine the virtual-mass effect of surrounding water.
5. To determine the effect of hydrostatic pressure on the resonance frequencies of lobar vibration.

For these tests two pairs of simplified models of submarine pressure hulls were tested. One model of each pair was subjected to hydrostatic pressure only, while the other model was subjected to combined hydrostatic pressure and steady-state lobar vibrations. The first set of models, designated DR201 and DR202,* failed by shell yield, while the second set,

*At the time of these tests Model SS-3U, a model identical to Model DR201 which was constructed by the Norfolk Naval Shipyard for explosion tests, had recently been subjected to hydrostatic tests at the Taylor Model Basin in connection with an investigation of residual strength.⁵ In general, repetition of this test would be considered desirable, but in this case funds were limited and duplication was not believed warranted for these exploratory tests. For these reasons the results obtained on SS-3U are used for comparison purposes in this report. The complete description and results of this phase of the test are given in Reference 5.

designated DR203 and DR204 and identical to the first set except for lighter frames, failed by general instability. The results of these four tests are contained in reports issued in two parts, Part I pertains to Models DR201 and DR202; Part II⁴ pertains to Models DR203 and DR204 and also contains a general discussion of all results.

In this report, Part I, there is contained a description of the models, instrumentation, test procedures, and model damage. Also included are results of static and dynamic strain measurements and of the measured resonance frequencies of the model in air, surrounded by water at atmospheric pressure, and as hydrostatic pressure is applied. The results are discussed and compared with appropriate theories for the static and dynamic behavior of a stiffened circular cylinder. From these discussions conclusions are drawn with a view toward satisfying the test objectives.

DESCRIPTION OF MODELS

The models tested simulate the center circular section of a submarine pressure hull with five evenly spaced rectangular frames and two heavy rings at each end which simulate wing bulkheads. The geometric characteristics of the models are:

$2R$	Diameter to the median surface of the shell	26.84 in.
h	Nominal thickness of the shell	0.156 in.
L_f	Center-to-center distance between adjacent frames	4.50 in.
L	Effective unsupported length of shell between frames	4.22 in.
L_b	Distance between external bulkhead rings	31.5 in.

Additional geometric characteristics of the models are given in Table 1. The nominal dimensions of the models are shown in Figure 1. The shells are constructed of 5/32-in. medium-steel plate.

The yield strength of the steel employed in Models DR201 and DR202 is not known exactly because the strength of samples of steels for a large number of similar models was measured by the manufacturer without correlating individual specimens and models.⁵ From the data later available it was learned that the values of yield strength could have varied between 37,000 and 44,000 psi. It is possible that a nominal value of the yield strength of 40,000 psi* could be used for Model DR202, and it is suspected that Model DR201 may have had a slightly higher yield strength—on the order of 43,000 to 44,000 psi.**

*The average value of yield strength from data furnished by the manufacturer for a large number of models which included Model DR202 was 40,000 psi.

**Tests of samples obtained from two other 5/32-in. plates in the manufacturer's stock at the time of construction of Model DR201, and later used for construction of Models DR203 and DR204, give a yield strength of 43,000 psi in the direction of mill roll (circumferential on models) and 44,600 psi normal to the direction of roll (longitudinal on models) with a Rockwell hardness of B-72.

TABLE 1

Geometric Characteristics of Models DR201, DR202, DR203, and DR204

Component	Characteristics		TMB Models DR201 and DR202 (Figure 1)	TMB Models DR203 and DR204 (Figure 1)	
Rectangular Frame Only	A	Cross-sectional area	in ²	0.211	0.131
	I	Moment of inertia for section	in ⁴	0.00987	0.00235
	I/A	Ratio of moment of inertia to cross-sectional area	in ²	0.468	0.018
	r	Radial distance from center to neutral axis of frame	in.	13.875	13.738
	r^4		in ⁴	3.706×10^4	3.562×10^4
	$A\gamma/g$	Mass per unit length of frame	$\frac{\text{lb-sec}^2}{\text{in.}}$	1.55×10^{-4}	0.958×10^{-4}
Shell Only	t	Thickness of shell	in.	0.156	0.156
	I	Moment of inertia of section for one frame spacing (4.5 in)	in ⁴	0.143×10^{-2}	0.143×10^{-2}
	r	Radial distance from center of cylinder to neutral axis of shell section	in.	13.422	13.422
	r^4		in ⁴	3.245×10^4	3.245×10^4
	$A\gamma/g$	Mass per unit area of shell	$\frac{\text{lb-sec}^2}{\text{in.}}$	1.14×10^{-4}	1.14×10^{-4}
Combined Shell and Frame (Assuming width of plating equal to one frame spacing to be effective)	L_f	Frame spacing	in	4.5	4.5
	A	Cross-sectional area	in ²	0.913	0.833
	I	Moment of inertia for combined section	in ⁴	0.0446	0.0144
	I/A	Ratio of moment of inertia to cross-sectional area	in ²	0.0489	0.0173
	r	Radial distance from center of model to neutral axis of section	in.	13.527	13.471
	r^4		in ⁴	3.348×10^4	3.293×10^4
	$A\gamma/g$	Mass per unit length of section	$\frac{\text{lb-sec}^2}{\text{in.}}$	6.69×10^{-4}	6.11×10^{-4}

For purposes of orientation of instrumentation and model damage, the circumference of the models is divided into degree orientations with the longitudinal seam at 180 deg measured clockwise looking into the open end. Frames are numbered consecutively from 1 to 5 from the open end to the closed end; the top bulkhead (open end) is designated as Bulkhead 1, and the bottom one as Bulkhead 2.

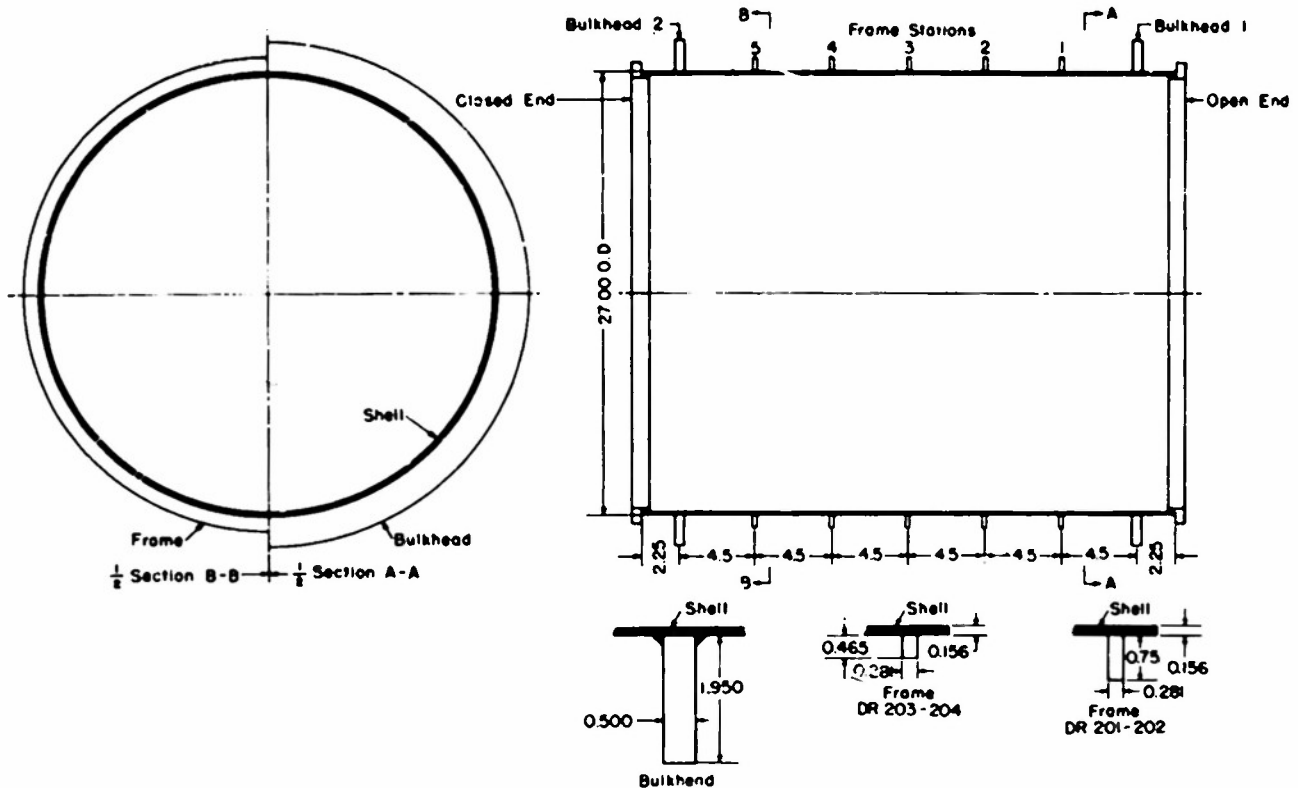


Figure 1 - Schematic Diagram of Models DR201, DR202, DR203, and DR204

The shells of Models DR201 and DR202 were constructed of 5/32-in. medium-steel plate, and the frames were constructed of high-tensile steel. The exact yield strength of the material used is not known but probably ranged from 37,000 to 44,000 psi.

INSTRUMENTATION AND TEST PROCEDURES

Both models were tested in the Taylor Model Basin 1500-psi, 37-in. diameter pressure tank. The bottom of each model was sealed by a welded pressure-tight bulkhead, and the top was welded to the serrated clamping ring for attachment of the model to the tank. The ring has a large opening which permits access to and visual observation of the interior of the model during test.

Circularity measurements were obtained at the frames and midway between the frames to indicate the initial out-of-roundness of both models and the final configuration after collapse. No further measurements applicable to this test were made on Model DR202.

To study static and dynamic response, Model DR201 was first loaded to a given increment of hydrostatic pressure, and the static strains and pressure were recorded. The model was then vibrated at the various modes of lobar vibration; the dynamic strains, the force applied by the vibration generator, and the dynamic pressure inside the test tank were recorded simultaneously on the moving film of a Consolidated electromagnetic oscillograph. This

sequence of loading and recording was adopted to minimize the possibility that large lobar strains might serve to strain-harden the model and thereby increase the pressure at which nonlinearity would occur.

The hydrostatic loading schedule was:

Pressure Increments, psi			
First Loading		Second Loading	
0	325	0	450
50	350	300	475
100	375	325	
150	400	350	
200	425	375	
250	450	400	
300	0	425	

In order to evaluate the mode shapes and resonance frequencies of the model subjected to lobar vibrations, data were obtained under the following conditions:

1. Model in air with test ends attached.
2. Model mounted in hydrostatic pressure tank surrounded by air at atmospheric pressure.
3. Model mounted in hydrostatic pressure tank surrounded by water at atmospheric pressure.
4. At each increment of hydrostatic pressure during test.

For producing the required radial excitation during combined loading tests two Calidyno electromagnetic generators, each capable of developing a maximum force of 25 lb, were attached to the structure at locations shown in Figure 2. Each shaker has a calibration of 3.1 lb/amp (rms) armature current with the field current to each shaker adjusted to 0.4 amp. The weight of the armature which is attached to the structure is 0.66 lb. For the tests conducted in air, where the additional force was not required, only one shaker was employed in order to minimize the inertia effect of the mass of the armature. Control apparatus consisted of a 115-v d-c field supply, a Hewlett-Packard 202D oscillator with a frequency range from 2 to 70,000 cps (which serves as the variable-frequency signal source), a 50-w power amplifier coupled to the calibrator through a variac (continuously variable auto-transformer), and an armature-current indicator. The armature-current signal was monitored on a cathode-ray oscillograph to check on the purity of the sine-wave excitation, and, in addition, the armature current was recorded together with the strains. A reversing switch inserted in the armature circuits enabled the respective phases of the two vibration generators to be changed for corresponding modes of lobar vibration. The resonance frequencies were determined by varying the frequency of the exciting force and noting the frequencies at which maximum structural response occurred for a minimum armature current at a given power setting.

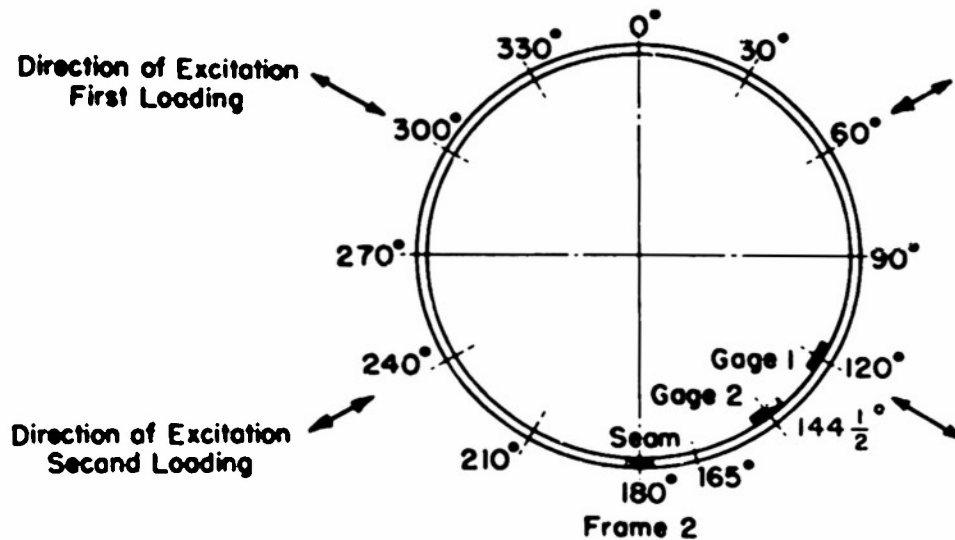


Figure 2a

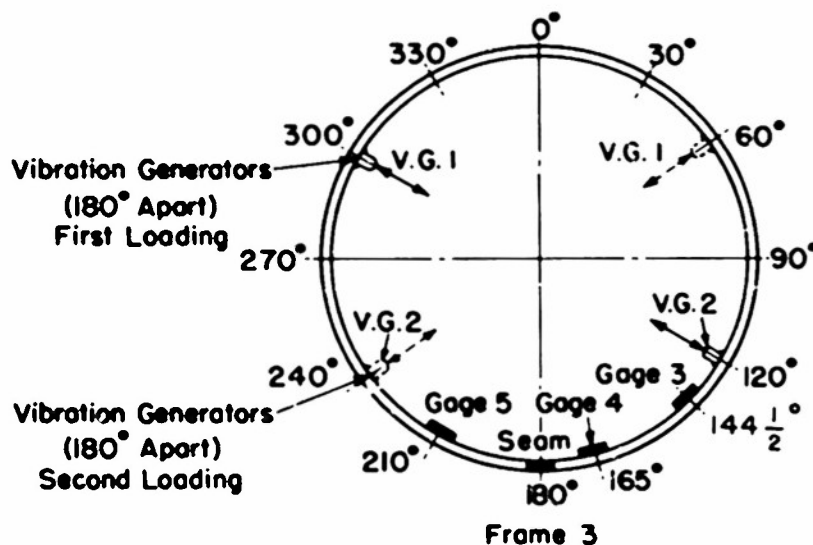


Figure 2b

Figure 2 - Location of Instrumentation on Model DR201

The vibration generators were connected to the interior surface of the shell, 180 deg apart, at Frame 3 and were located at 120-deg and 300-deg orientation for the first loading. They were relocated at 60-deg and 240-deg orientation for the second loading.

As noted in Figure 2 the locations of the vibration generators were changed between the first and second loading. This change in location was not originally planned and was due to observations made during the test. It was noted during the first loading that at the 425-psi increment a small bulge* occurred at 40-deg orientation between Frames 2 and 3.

*The bulge consisted of a single lobe resembling that developed by shell instability; this was believed occasioned by local plastic yielding of the shell material which resulted in a reduction in equivalent modulus of elasticity causing buckling of the shell.

Collapse was then believed imminent, but pressure was increased to 450 psi without further suggestion of failure. Arrest of this local yielding was attributed to strain hardening, and as a result it was then decided to reorient the vibration generators to give maximum lobar excitations at a different location. Hence, during the first loading the vibration generators were connected to the interior surface of the shell 180 deg. apart at Frame 3 at 120-deg. and 300-deg. orientation; for the second loading the vibrators were relocated at 60-deg. and 240-deg. orientations.

In order to obtain the circumferential dynamic strain distribution around the shell and the superposed static strain, Type A-7, SR-4 strain gages were mounted at the five locations shown in Figure 2. To facilitate testing and analysis, separate gages were mounted at each location for simultaneous measurement of static and dynamic strain; each gage was connected directly to equipment most suitable for recording the respective measurement. The static gages were connected to a Baldwin Southwark, Type K, strain indicator for which a dummy temperature-compensating gage was mounted on an unstressed piece of steel attached inside the model. Each active dynamic gage employed a separate dummy gage, and the two were connected so as to form two arms of a bridge circuit. These gages were connected to a TMB 5K15-A strain indicator, a carrier-type instrument for use in measuring dynamic strains at frequencies up to 1000 cps. The instrument is designed for use with Type A SR-4 wire-resistance strain gages and will deliver up to 15 ma to a 7-ohm galvanometer for strains from 100 to 6000 μ in/in. Internal calibration is provided for each sensitivity step. A Consolidated electromagnetic oscillograph with 10-ma galvanometers was used to record the dynamic strains. A 60-cycle timing signal was impressed upon one galvanometer to serve as a time base.

Both the hydrostatic pressure and the variation of pressure within the test chamber while the model was being vibrated were recorded. The hydrostatic pressure was measured with a 1000-psi Bourdon-tube pressure gage. Since it was expected that the change in volume within the test chamber due to vibration of the model would be small, it was necessary to select a pressure gage that could withstand the maximum hydrostatic pressure and yet be sensitive enough to record the small variations in pressure. The most suitable instrument readily available which would satisfy these conditions was a TMB 1000-psi elastic-tube pressure gage, which consists essentially of a thin elastic steel tube with strain-sensitive electrical wire attached to it. This gage has a sensitivity of 0.7 μ in/in/psi. The signal input from this gage was fed into a TMB 5K15-A strain indicator and recorded on the Consolidated oscillograph, thus enabling the variation in pressure to be recorded to the nearest pound per square inch.

RESULTS

It will be recalled that Model DR202 was tested in connection with residual-strength studies⁵ and was not instrumented with strain gages. The model failed at a pressure of 515 psi by shell yield. Figure 8 shows that maximum damage occurred between Bulkhead 1 and Frame 1 and in the bay between Frame 1 and Frame 2. Plots of initial circularity before testing and final contours after collapse are shown in Figures 4 and 5.



Figure 8 - Model DR202 after Hydrostatic Test

Note failure by yielding of the shell at 515 psi accompanied by plastic instability of shell (formation of lobes).

Before presenting the results for Model DR201 in detail, it is significant to recall that a shell bulge in this model was observed at 425 psi at 40-deg orientation between Frames 2 and 3. This occurred during vibration of the model at $i = 4$ or $i = 5$ mode. As previously mentioned the hydrostatic pressure was then increased to 450 psi, and the model was again vibrated but collapse did not occur. The test was then repeated for the second loading sequence, and the model failed as hydrostatic loading was being applied at 495 psi with a shell-yield type of failure accompanied by plastic instability (formation of lobes).

Major damage to Model DR201 resulting from final collapse at 495 psi occurred between Bulkhead 1 and Frame 1 and extended continuously around the model for approximately

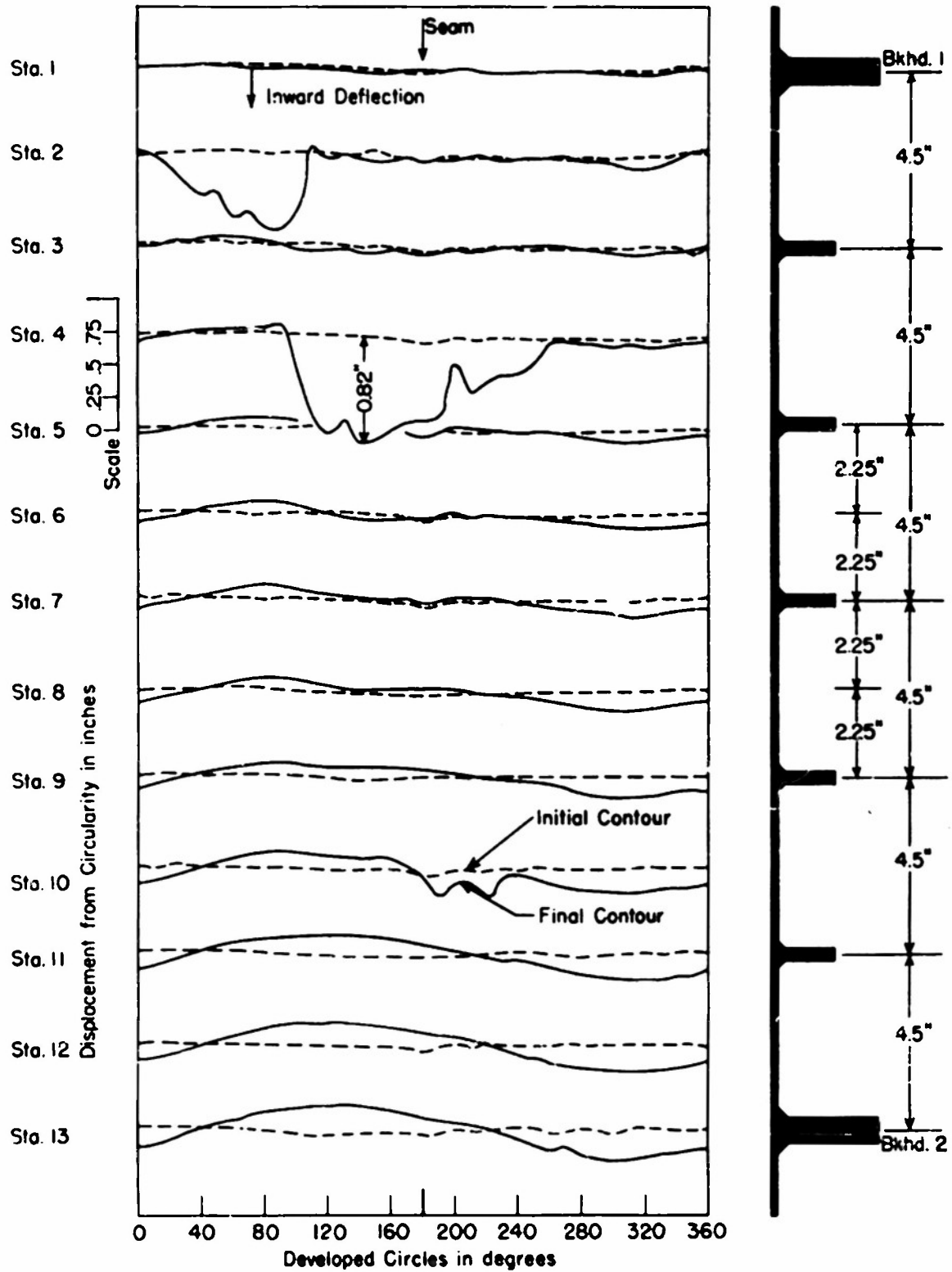


Figure 4 - Displacement from Circularity of Model DR202

Final contours were made after initial failure; subsequently pressure was applied to enlarge area of damage as shown previously in Figure 3.

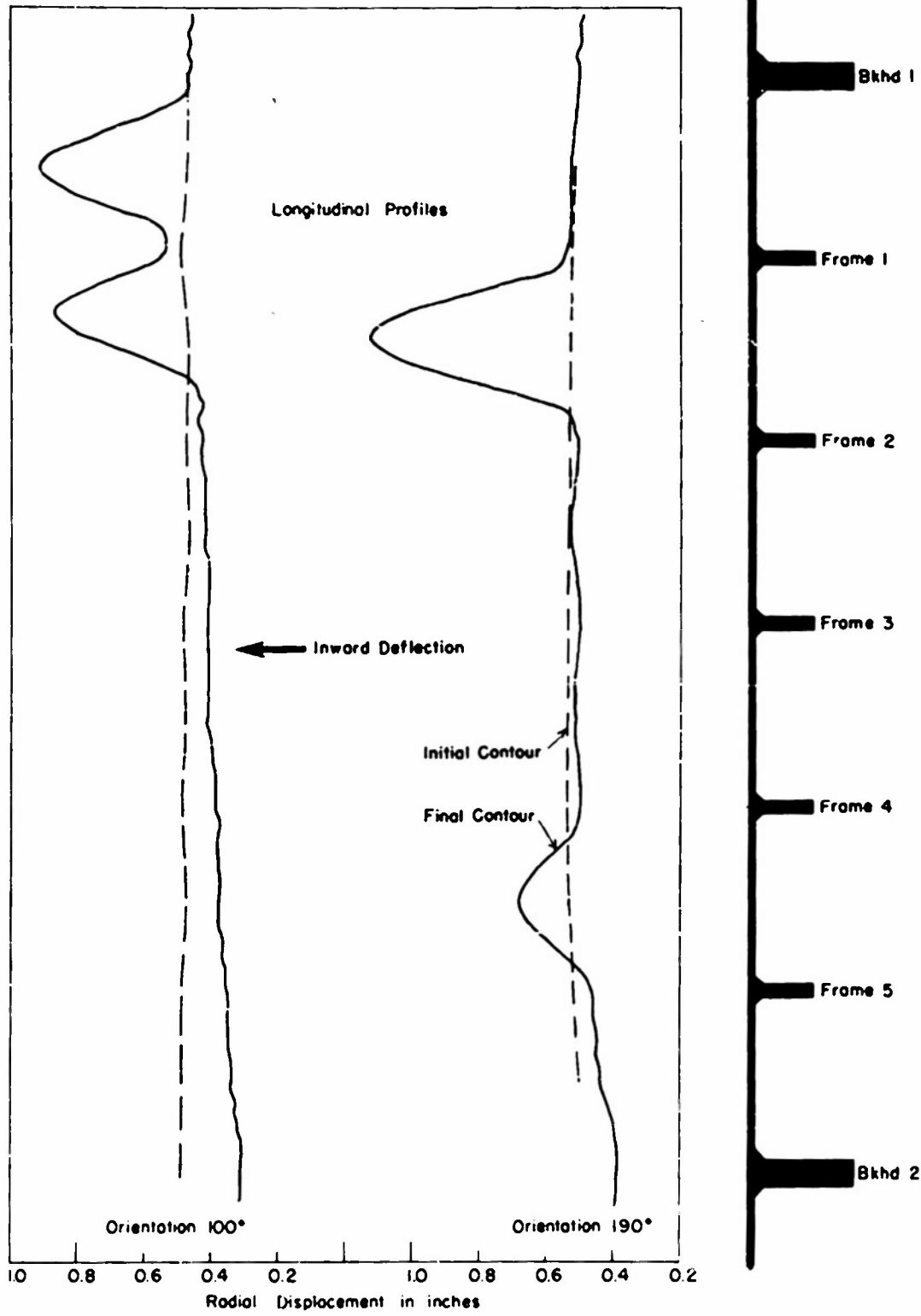


Figure 5 - Longitudinal Profile of Model DR202 through Maximum Bulge

170 deg on both sides of zero orientation from 0 to 110 deg and from 300 to 360 deg. Figure 6 shows the damage as seen looking into the interior of the model when it was still mounted in the hydrostatic test tank. Exterior views of the damaged model removed from the test tank with end mounting plates still attached are shown in Figure 7.

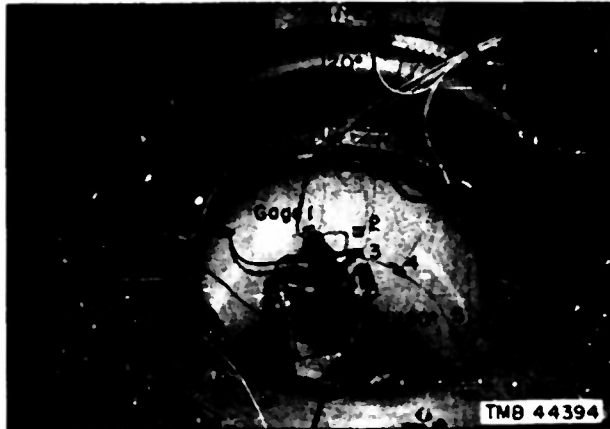


Figure 6a - Before Collapse, First Loading

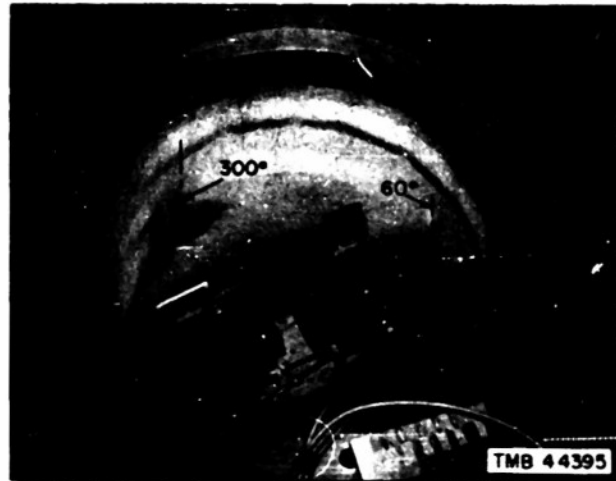


Figure 6b - After Collapse, Second Loading

Figure 6 - Interior View of Model DR201

The model is still mounted in the hydrostatic test tank, and test apparatus is still in place. Note failure by yielding of the shell at 495 psi accompanied by plastic instability (formation of lobes) in Figure 6b.



Figure 7a

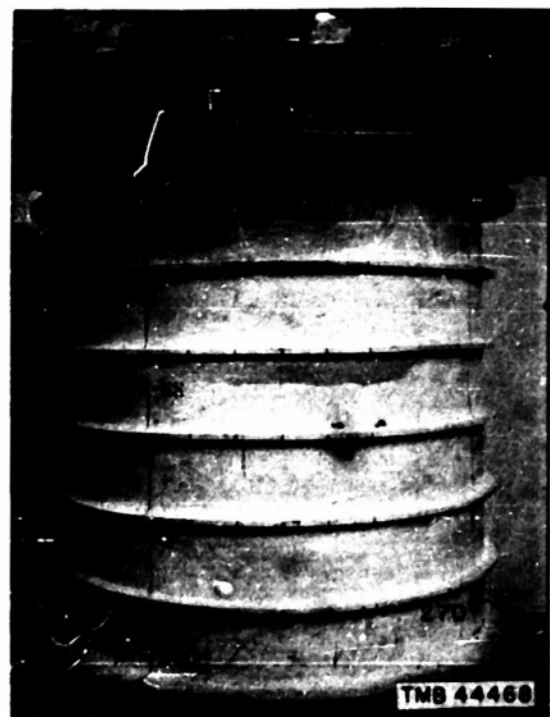


Figure 7b

Figure 7 - Exterior View of Model DR201 after Collapse

The model has been removed from the test tank, but the end mounting plates are still attached.

A quantitative evaluation of the initial circularity and the final damaged shape may be obtained by examining the circularity charts. A typical circularity chart is shown in Figure 8; the complete circularity data may be found in Figures 18 to 80 in the Appendix. Circumferential and longitudinal profiles for the initial and final deflections in the region of greatest

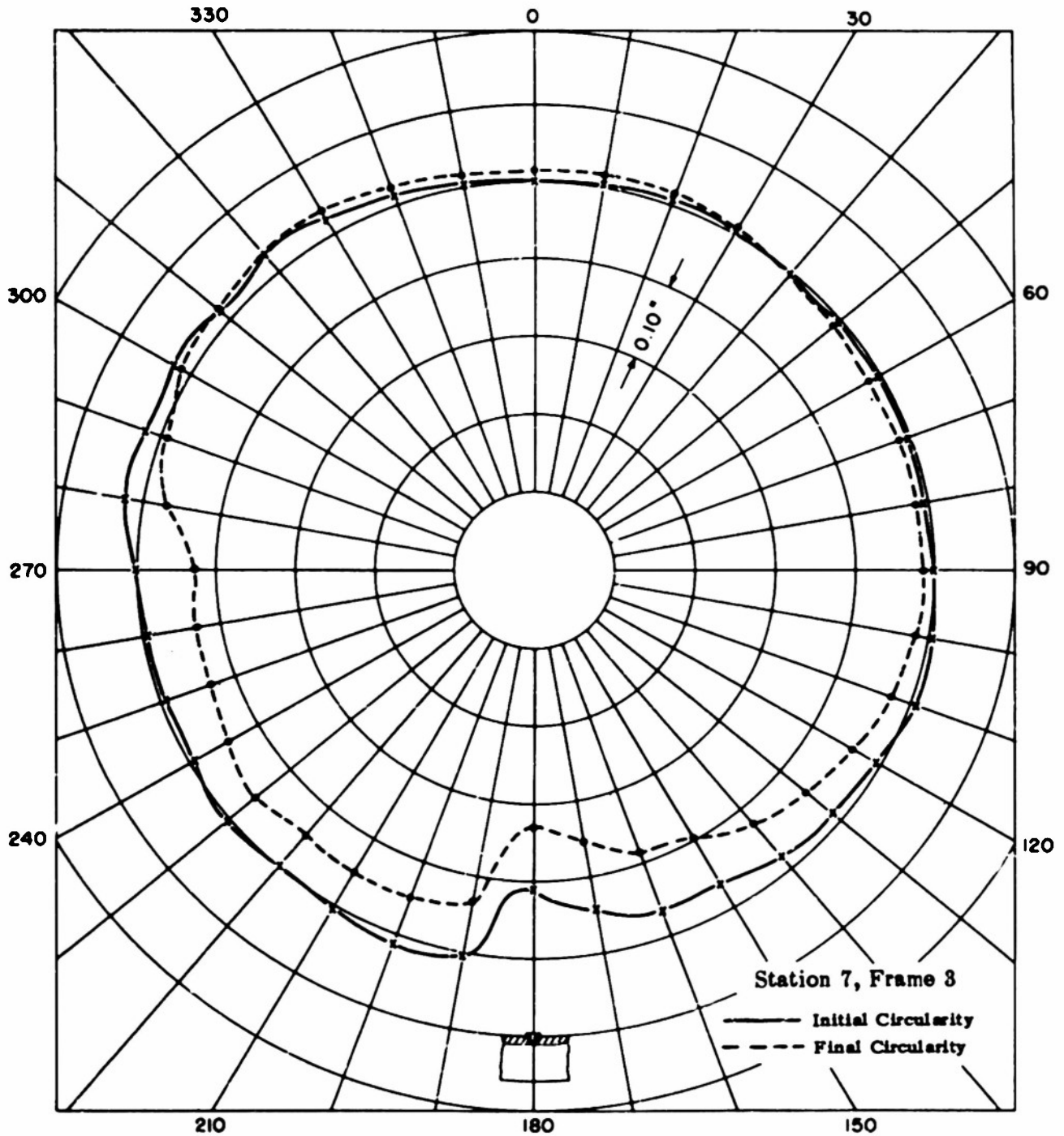


Figure 8 - Typical Circularity Chart for Model DR201

damage are shown in Figure 9. The initial circularity of the model is within the specified tolerances for out-of-roundness with the exception of one location at the longitudinal seam, Frame 3, as shown in Figure 8. Here the maximum initial deviation from an approximate mean true radius is 0.09 in., which is slightly greater than the one-half shell thickness allowed by specification.

The static strain measurements are given in Figure 10. These curves indicate that some yielding occurs between 200 and 300 psi during the first loading. For purposes of evaluation, the reciprocal of the slopes of the linear portion of these curves for the final loading is given as a strain sensitivity coefficient in microinches per inch per psi. It is noted that some variation in strain sensitivity occurs around the circumference of the model. This variation, which has been observed in similar models, could possibly be attributed to small abrupt local variations

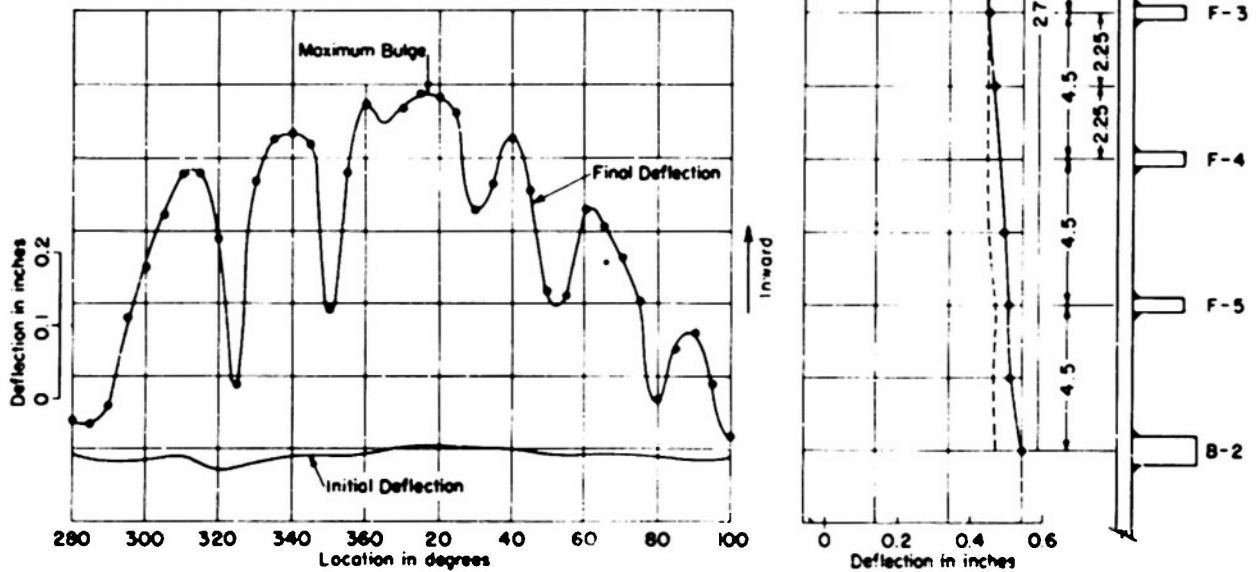


Figure 9 - Circumferential and Longitudinal Deflection Profiles in the Region of Greatest Damage to Model DR201

The circumferential profile was obtained midway between Bulkhead 1 and Frame 1. The longitudinal profile was obtained at 15-deg orientation.

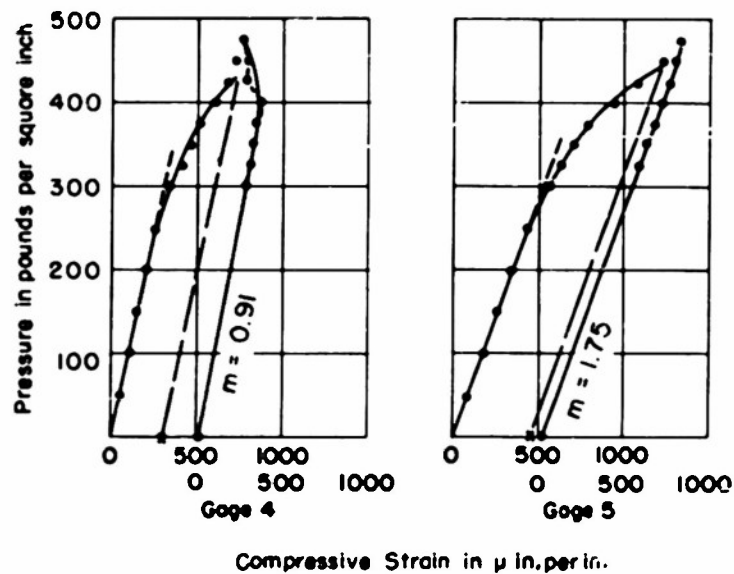
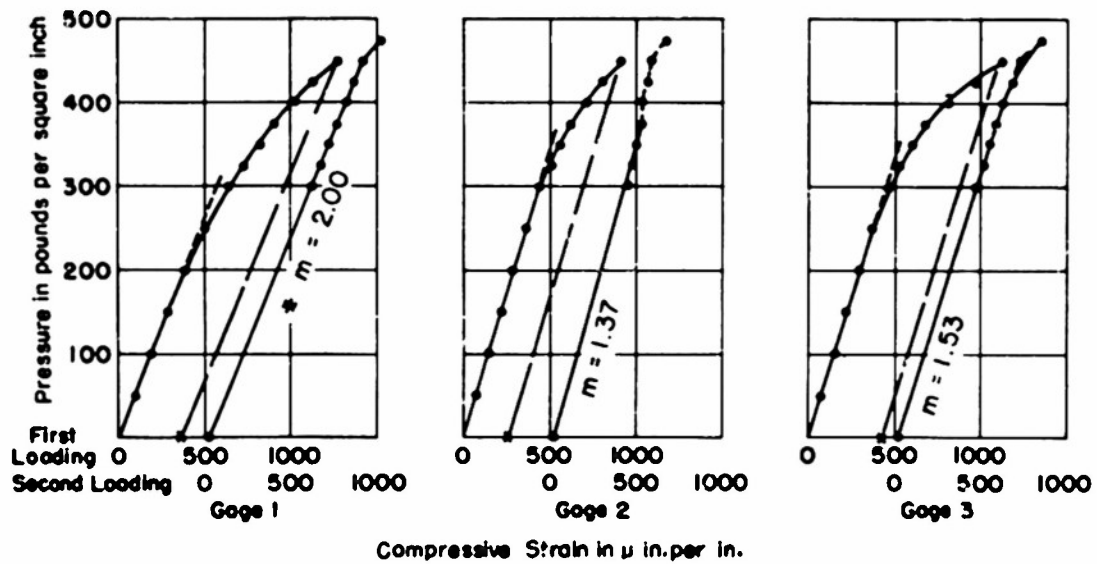


Figure 10 - Results of Static Strain Measurements on Model DR201 Plotted as a Function of Hydrostatic Pressure

α = strain sensitivity coefficient μ in/in/psi.

By averaging the above strain sensitivity coefficients, a mean value of 1.51 μ in/in/psi is obtained.

in circularity and shell thickness although this has not been conclusively shown. Hence, for comparison with computed static strains, the experimental observations were averaged and a value of $1.51 \mu \text{ in/in/psi}$ was obtained.

Tabulated results of the dynamic tests for the first and second loadings are given in Tables 2 and 3; these show the amplitude of driving force due to the vibrator, the resonance frequencies, and the resulting dynamic strain at each gage location for every increment of hydrostatic load for the various lobar modes. The modes excited were $i = 3$, $i = 4$, and $i = 5$; the $i = 2$ mode could not be excited with the model clamped in the test tank. In examining the tabulated data, it should be noted that during the first loading sequence up to 425 psi the strains measured by Gage 1 represent the maximum for each mode. This is not true for the second loading due to reorientation of the vibration generators. However, the consistency of the data for both loadings is indicated by comparison of strains measured by Gages 2 and 3 located at the same circumferential orientation one frame spacing apart. Gage 3 gives a slightly higher value of strain than Gage 2 due to larger displacements at this location.

Summarized values of dynamic strain sensitivities, microinches per inch per pound dynamic force plotted against hydrostatic pressure for $i = 3, 4$, and 5 modes of lobar vibration for Gage 1 during the first loading, are shown in Figure 11. From these results it appears,

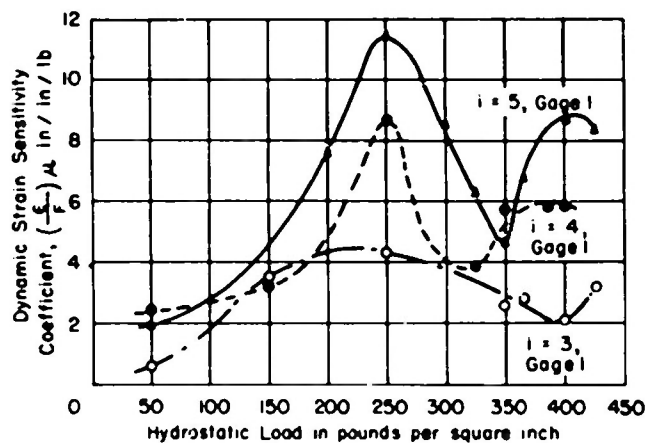


Figure 11 - Summarized Values of Dynamic Strain Sensitivities (Unit Strain per Pound Applied Force) Plotted against Hydrostatic Pressure for Various Lobar Modes, First Loading of Model DR201

in general, that the dynamic strain sensitivity increases for each successive higher mode measured and, also, as the hydrostatic pressure is increased up to 250 psi. Above this value of hydrostatic load, the relationship between dynamic strain sensitivity and hydrostatic pressure decreases and then slightly increases again. As will be shown later this behavior cannot be rationally related to the structure of the model itself, and several explanations have been sought from examination of the test conditions.

The dynamic variation in pressure within the hydrostatic test chamber while the model was being vibrated was small, less than 3 psi, and can be considered negligible as a contributor to failure. This is as would be expected since the change in volume due to the inextensional component of vibration would necessarily be small.

TABLE 2

Results of Dynamic Measurements During Combined Loading Test,
First Loading, Model DR201

Hydrostatic Pressure psi	Driving Force, lb Single Amp.	Resonance Frequency cps	Dynamic Strain μ in/in Single Amplitude				
			Gage 1	Gage 2	Gage 3	Gage 4	Gage 5
Lobar Mode $i = 3$							
50	22	247	12	17	18	8	16
100	20	242	35	28	28	66	45
150	26	247	90	107	112	77	93
200	30	246	106	130	174	143	94
250	22	237	94	85	89	178	135
300	25	242	47	58	60	-	34
325	26	242	93	105	112	85	67
350	26	233	67	46	53	109	92
365	24	233	66	46	52	105	111
400	25	227	52	44	42	90	72
425	20	227	64	46	53	107	90
450	20	228	52	46	42	97	76
Lobar Mode $i = 4$							
50	11	325	25	13	16	15	34
100	11	326	181	52	70	128	-
150	25	320	80	35	37	103	109
200	24	315	140	32	19	143	159
250	31	315	260	108	111	303	333
300	24	309	32	9	9	46	38
325	24	303	90	18	17	106	108
350	22	301	126	75	79	160	164
365	24	300	136	69	78	180	176
400	20	301	106	75	85	113	139
425	22	296	142	80	56	177	192
450	20	293	127	69	80	151	158
Lobar Mode $i = 5$							
50	14	472	27	9	9	31	8
100	20	472	212	70	80	16	-
150	22	465	69	27	26	78	127
200	21	457	160	98	105	173	21
250	16	455	183	94	100	165	21
300	13	446	110	74	77	86	34
325	24	440	151	90	98	120	35
350	20	437	93	62	60	73	25
365	17	434	112	80	82	90	28
400	13	433	113	74	85	86	35
425	17	428	143	126	105	106	47
450	19	427	136	89	97	108	40

TABLE 3
Results of Dynamic Measurements During Combined Loading Test,
Second Loading, Model DR201

Hydrostatic Pressure psi*	Driving Force, lb Single Amp.	Resonance Frequency cps	Dynamic Strain μ in/in Single Amplitude				
			Gage 1	Gage 2	Gage 3	Gage 4	Gage 5
Lobar Mode $i = 3$							
0	31	243	32	32	37	72	51
325	26	233	78	46	42	115	98
375	23	233	83	60	61	131	64
400	27	232	68	57	56	136	101
425	26	230	94	80	81	161	131
450	24	228	64	55	55	119	104
475	22	227	70	59	63	130	164
Lobar Mode $i = 4$							
0	23	332	7	68	76	13	14
325	31	306	87	52	51	138	95
350	22	304	77	60	66	95	89
375	20	299	32	183	187	39	49
400	26	298	31	195	219	137	38
425	27	295	28	189	222	33	44
450	29	293	38	135	154	65	61
475	22	290	29	115	135	32	34
Lobar Mode $i = 5$							
0	19	480	71	19	19	79	29
325	23	443	227	44	36	316	98
350	23	439	291	60	52	365	129
375	25	437	185	30	27	224	79
400	26	437	170	56	32	192	64
425	28	432	129	40	41	143	35
450	23	428	112	35	38	122	23
475	22	425	93	35	39	100	17

*Measurements at atmospheric pressure obtained after collapse.

The change in the lobar resonance frequencies plotted as a function of hydrostatic pressure is shown in Figure 12. It is noted that the resonance frequency for each mode is diminished as the hydrostatic loading is increased.

Table 4 lists the observed resonance frequencies obtained on Model DR201 under the various test environments and also shows the effect of hydrostatic pressure and virtual mass of surrounding water on the resonance frequencies of lobar vibration. Here it is noted that the resonance frequencies in water are only about 60 percent as large as those obtained in air due to the virtual-mass effects of the surrounding water, and furthermore, that increasing the hydrostatic pressure lowers the resonance frequencies still further.

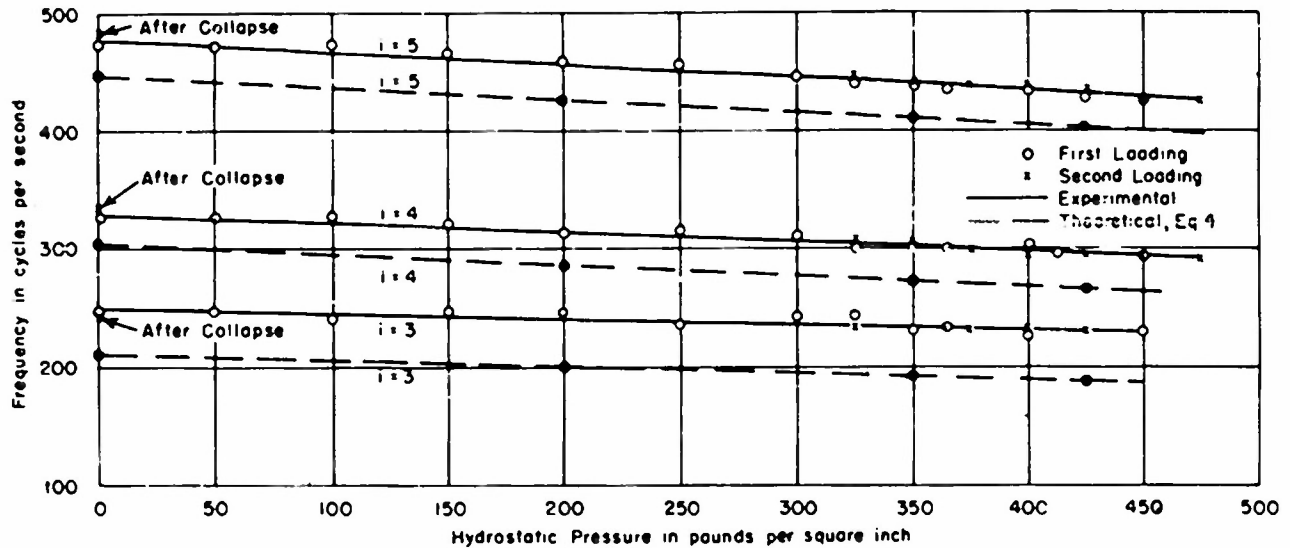


Figure 12 - Experimental and Theoretical Variation of Resonance Frequencies of Lobar Vibration with Hydrostatic Pressure for Model DR201

The dotted curve was obtained from Equation [4], page 30, which incorporates the theoretical effects of virtual mass and hydrostatic pressure into the frequency equation of an elastically supported ring. Experimentally determined values of $\xi = 3.35 \times 10^4$ and $\eta = 626 \times 10^4$ for the model in air were used.

TABLE 4

Observed Frequencies of Lobar Vibration Obtained under Various Test Environments

The amount by which the resonance frequencies of lobar vibration are lowered because of the virtual mass of surrounding water varies slightly from 43 percent at $i = 3$ to 59 percent at $i = 5$.

Test Environment	Frequency, cps				
	First Flexural Mode $i = 2$	Second Flexural Mode $i = 3$	Third Flexural Mode $i = 4$	Fourth Flexural Mode $i = 5$	Fifth Flexural Mode $i = 6$
Model in Air	365	440	580	790	1020
Model Mounted in Pressure Tank Surrounded by air at atmospheric pressure	-	485	590	790	-
Surrounded by water at atmospheric pressure	-	250	330	480	-
Surrounded by water at 200 psi	-	246	315	457	-
Surrounded by water at 350 psi	-	233	301	437	-
Surrounded by water at 425 psi	-	227	296	428	-

DISCUSSION OF RESULTS

The occurrence of an initial shell bulge, observed on Model DR201 at 425 psi, well in advance of final collapse pressure (495 psi) has not been observed previously during hydrostatic tests of models and is attributed to the presence of lobar vibration. It is impossible to know whether or not collapse would have occurred at this time had the pressure been maintained, i.e., the condition of a pressure hull surrounded by an infinite fluid medium.*

The observed difference between final collapse pressures for Models DR201 and DR202 (495 and 515 psi) was small but would have been somewhat larger if models having shell material of the same yield strength had been used. The lack of exact information concerning the yield strength masks the results considerably. However, it is possible to deduce from the measurements obtained that the reduction in collapse pressure for this model, designed to fail by shell yield, might be attributed to superposition of dynamic stresses upon hydrostatic stresses.

Correlations between experimental and theoretical stresses and collapse pressures serve to amplify the above statements. Qualitative comparisons can be made by employing a nominal value of 42,000 psi for yield strength. Using standard practice of equating the elastic stress of Formula 92a (from theory of von Sanden and Gunther⁶) to the yield stress of material, the collapse strength of the model is 490 psi. With the elastic stress at the median surface of shell midway between frames (from the same theory) equal to the yield strength given by the von Mises-Hencky⁷ theory of failure, the collapse strength is 602 psi.** It is not yet known which method of computing collapse pressure is valid. However, for the purpose of demonstrating the effect of superposing the static and dynamic stresses, the first method of calculation is employed. From Table 3, it is noted that during combined loading

*Under this condition the shell could conceivably displace until strains of sufficient magnitude would initiate strain hardening which would result in a rapid deceleration of the structure. The subsequent response may be considered analogous to the magnified response of an elastic structure under dynamic loading.

**It is also noted that the Salerno and Levins⁸ theory indicates that general instability failure would occur at 675 psi with an $i = 4$ mode of collapse by assuming simple end support and at 924 psi with an $i = 5$ mode of collapse with clamped ends.

of Model DR201, the maximum dynamic circumferential strain was of the order of $150 \mu\text{in/in.}$, which corresponds to a uniaxial stress of 4500 psi. Superposition of this stress upon hydrostatic stress reduces the above computed collapse pressure from 490 psi to 435 psi. This serves to indicate that superposition of stresses can account for the lowered pressure at which the first bulge occurred and might in turn account for the difference in final collapse pressures. An explanation for reductions in collapse pressures for models which fail by general instability will be discussed in Part II of this report.⁴

A further comparison of the von Sanden and Gunther elastic theory with experiment may be obtained from examination of the circumferential and longitudinal strain distributions shown in Figures 13 and 14. It is seen from Figure 13 that the circumferential strain sensitivity directly under the frame, $x/l = 0$, of $1.58 \mu\text{in/in/psi}$ compares favorably with the average experimental circumferential hydrostatic strain at this location of $1.51 \mu\text{in/in/psi}$.

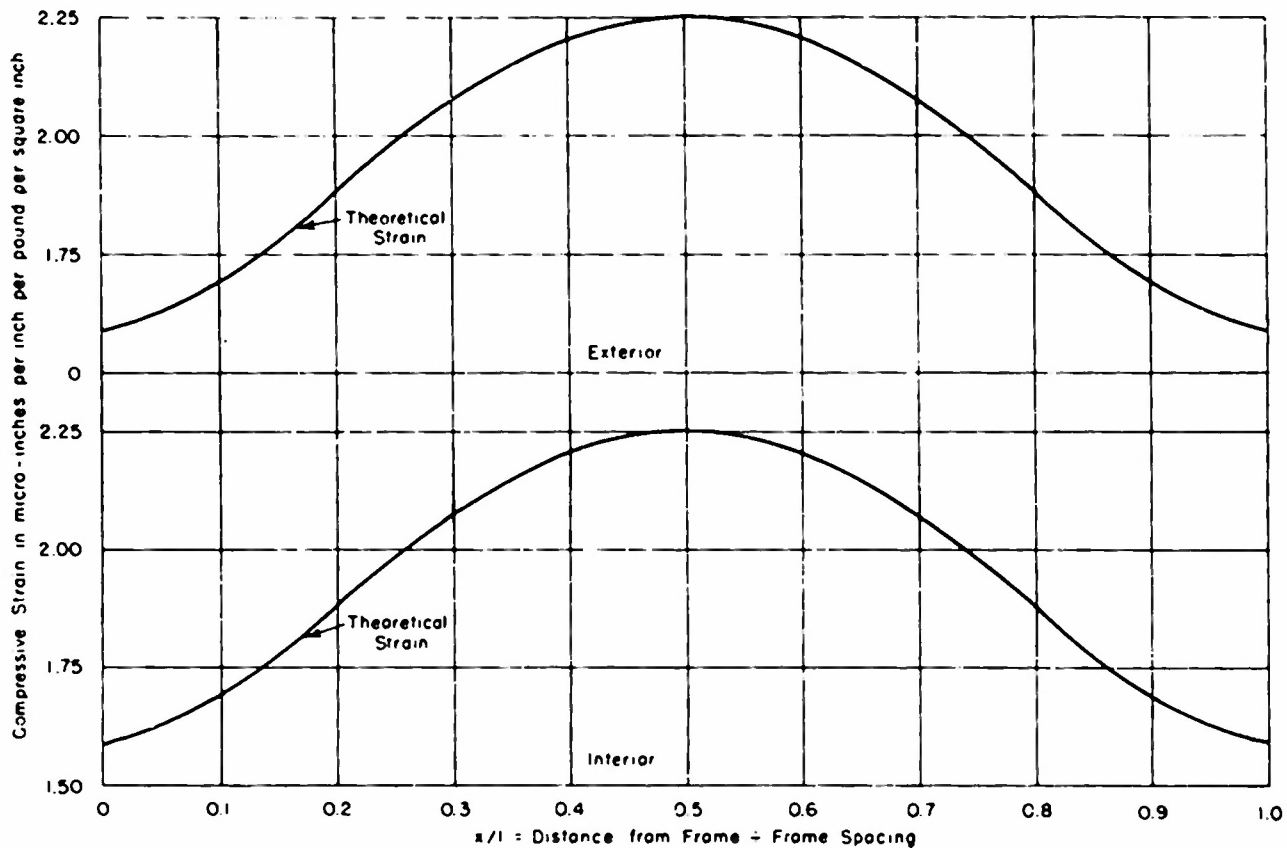


Figure 18 - Theoretical Circumferential Strain Distribution per Unit Hydrostatic Pressure for Models DR201 and DR202

The circumferential strain on the interior and exterior surfaces are identical.

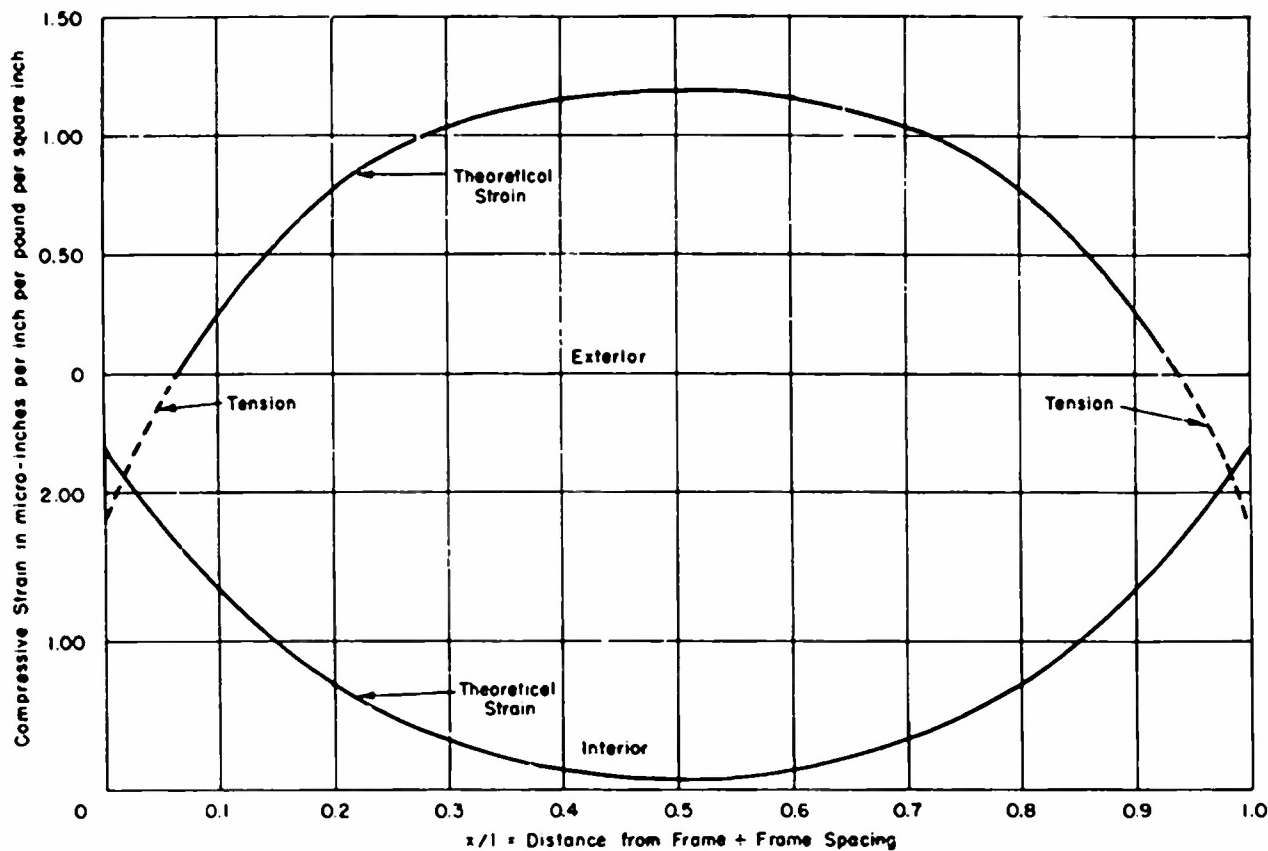


Figure 14 - Theoretical Longitudinal Strain Distribution per Unit Hydrostatic Pressure for Models DR201 and DR202

From inspection of the final collapse damage of Models DR201 and DR202, it can be observed that lobes are formed similar to the type expected by shell instability failure except that they are not formed completely around the circumference. It is postulated that, for these models having a thinness factor of

$$\lambda = \sqrt[4]{\frac{(L/2R)^2}{(h/2R)^3}} \sqrt{\frac{\sigma_y}{E}} = 0.77$$

plastic yielding of the shell material results in a reduction in equivalent modulus of elasticity causing buckling of the shell. This appears to be a possibility since there is a definite relation between the wave length of the lobes observed and those theoretically predicted for instability of tubes loaded with both radial and axial pressure by von Mises, Equation [6]. Reference 9. For the geometry of these models, $L/2R = 0.157$ and $h/2R = 0.0058$, von Mises predicts that 12 lobes would be formed for a shell instability mode of failure. The number of lobes observed for Model DR201 for 180 deg (Figure 9) is 6; this indicates that, if lobes were formed around the entire circumference as is assumed in the theory, there would have been 12 lobes.

As previously stated, the mode of vibration excited involved bending of the frame-and-shell combination in transverse planes such that longitudinal corrugations occur which vary sinusoidally in amplitude between holding bulkheads. During the test, prior to recording data, surveys of the relative amplitudes of vibration were made around the circumference of the model to define the modes of lobar vibration. The dotted curves in Figures 15 to 17 represent

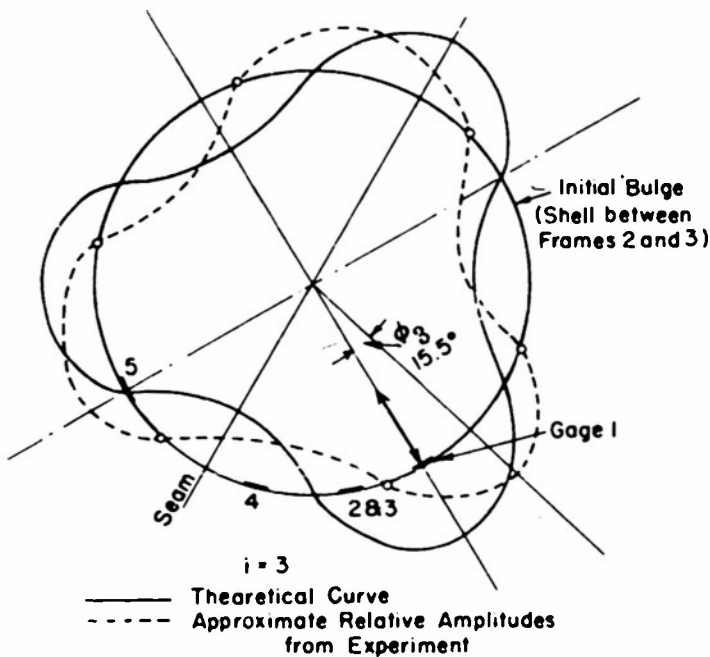


Figure 15 - Theoretical and Experimental Relative Radial Amplitudes of Lobar Vibration, $i = 3$ Mode, for Model DR201

The relative amplitudes are shown in relation to gage orientation and location of vibration generator.

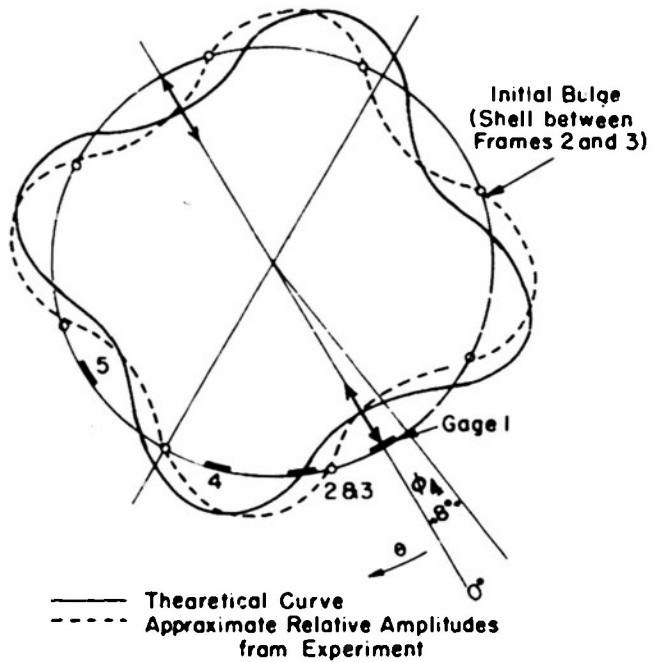


Figure 16 - Theoretical and Experimental Relative Radial Amplitudes of Lobar Vibration, $i = 4$ Mode, for Model DR201

The relative amplitudes are shown in relation to gage orientation and location of vibration generator.

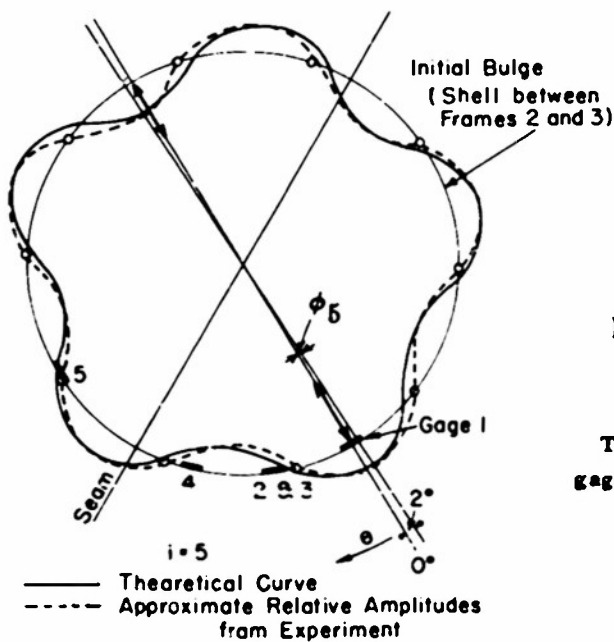


Figure 17 - Theoretical and Experimental Relative Radial Amplitudes of Lobar Vibration, $i = 5$ Mode, for Model DR201

The relative amplitudes are shown in relation to gage orientation and location of vibration generator.

the results of these surveys for $i = 3, 4, \text{ and } 5$ modes of excitation, while the solid lines show the theoretical amplitude distribution with reference to the orientation of the vibration generators and strain gages. It is noted that the experimental lobar-mode shapes around a circumference approximate those predicted by thin-ring theory except that the nodal points are shifted slightly and are not exactly equidistant. These discrepancies are probably due to the effects of added mass of vibration generators and experimental errors in locating exact nodal points. The mode shapes of lobar vibration are also reflected by the measured dynamic strains. Table 5 gives the ratios of measured strains (Gage 1/Gage 2, Gage 2/Gage 3, etc.) at $i = 3, 4, \text{ and } 5$ modes for three different pressure increments and compares these ratios with those predicted by thin-ring theory. In order to make this comparison, it is necessary to obtain theoretical ratios of moment at each gage location with reference to the observed peak amplitude in closest proximity to the point at which the force was applied (Figures 15 to 17) by assuming that moment distribution is given by $\cos i (\theta_n + \phi_i)$ where θ_n is the angular distance from Vibration Generator 1 to Gage n and ϕ_i is the distance between experimentally observed maximum amplitude and theoretical maximum at point of application of driving force. The comparison is very good considering that experimental nodes are not exactly equidistant and that location of the reference maximum is subject to experimental error of ± 3 deg. In addition this comparison serves to indicate that hydrostatic pressure does not significantly alter the mode shape.

TABLE 5
Comparison of Experimental and Theoretical Relative Values of Dynamic Circumferential Strains for Various Lobar Modes, Model DR201

	Relative Values of Strain			
	Gage 1	Gage 2	Gage 3	Gage 4
	Gage 2	Gage 3	Gage 4	Gage 5
	Lobar Mode $i = 3$			
Experimental				
at 250 psi	1.1	1.0	0.5	1.3
at 365 psi	1.4	0.9	0.5	1.0
at 450 psi	1.1	1.1	0.4	1.4
Theoretical	1.7	1.0	0.4	1.4
	Lobar Mode $i = 4$			
Experimental				
at 250 psi	2.2	1.0	0.4	0.9
at 365 psi	2.0	0.9	0.4	1.0
at 450 psi	1.8	0.9	0.5	1.0
Theoretical	1.6	1.0	0.6	1.0
	Lobar Mode $i = 5$			
Experimental				
at 250 psi	1.9	0.9	1.0	8
at 365 psi	1.4	1.0	0.9	3.2
at 450 psi	1.5	0.9	0.9	2.7
Theoretical	1.8	1.0	0.9	3.5

The observed cyclic variation in dynamic strain sensitivity with hydrostatic pressure shown in Figure 11 is not compatible with that which would be expected. Ordinarily, it would be presupposed from elementary theory that the dynamic bending strains per unit applied force would steadily increase as hydrostatic pressure is applied.* In reviewing the possible causes for this inconsistency, it was noted that by touching the test tank during the test a small amount of vibration was detected. This transmission of the model vibration through the serrated clamping flange to the test tank indicates that some of the energy was being dissipated because of the coupling action. In order to avoid possible effects of end constraint and associated coupling action, future tests of models of similar geometry will be conducted in the recently constructed 8-ft diameter tank, and the model will not be mechanically attached to the tank. An additional difficulty was encountered during the test which would affect the value obtained for dynamic strain sensitivity coefficient. Owing to the small amount of damping in the test structure, it was very difficult to obtain data at the very peak of the resonance curve for each mode. Any slight variation in the point on the resonance curve at which data were taken from one increment of loading to the next would produce an appreciable variation in the developed strain. In order to minimize this effect, the frequency was varied quite slowly near resonance, and recordings were made only when simultaneous observation of dynamic strain was a maximum and armature current (force) of monitored undistorted sinusoidal wave form was a minimum.

COMPARISON OF OBSERVED AND COMPUTED RESONANCE FREQUENCIES

An exact mathematical analysis has as yet not been generally accepted for the lobar vibrations of stiffened cylindrical shells with end bulkheads. Work on this subject is currently being conducted at Columbia University under Contract Nonr 266(08) by Bleich^{10,11} and at Harvard University by Junger.¹² Correlation of the experimental frequencies can also be obtained by considering the stiffened shell analogous to a collection of identical rings provided with elastic support by the shell.³ A complete theory for purposes of submarine design should make possible computation of the resonance frequencies of a stiffened cylindrical shell in air, in water at atmospheric pressure, and in water with hydrostatic loading. In addition, it should make possible calculation of displacements and bending moments for arbitrary loadings of steady-state or transient nature under the above conditions. A brief discussion of the comparison of available theory with experiment will serve to indicate current progress in this direction.

*This can be shown by considering the elementary case of a pin-connected beam subjected to a combined axial and lateral force as discussed by Timoshenko. The expressions for maximum lateral deflection and bending moment contain two factors; the first represents a deflection or bending moment caused by the lateral load alone while the second is a "magnification factor" representing the action of the axial force. For a very small axial force, the magnification factor is near unity, but as the axial force is increased the deflection and bending moment increase until ultimately at the critical load they increase without limit.

Results of theoretical correlation of the experimental frequencies obtained by considering the stiffened shell analogous to a collection of identical rings provided with elastic support by the shell are shown in Table 6 for the model in air and also when surrounded by water at atmospheric pressure. These results indicate that such an analogy is possible for the particular model geometry in question by assuming only radial elastic support. A similar correlation was attempted assuming combined radial and tangential elastic support but was not applicable since small negative values of tangential support were required to satisfy experimental observations. The introduction of a negative value for elastic support would imply that energy was being fed into the system by the elastic support, which is impossible. It is interesting to note, however, that the assumption of tangential support gives a higher value for the resonance frequency at $i = 2$ mode than at $i = 3$. Phenomena of this type noted in other tests have been regarded as a higher-order response because the second and higher $i = 2$ mode has always exhibited a weaker response to a given driving force. On the basis of observations made during these tests, in particular the inability to excite an $i = 2$ mode with the model mounted in the test tank, it appears that the additional but apparently secondary modes of response should be studied carefully in the future.

TABLE 6

Comparison of Experimental Frequencies of Lobar Vibration of Model DR201 in Air and in Water with Test Ends Attached with Frequencies Computed for an Elastically Supported Ring

	Frequency, cps				
	First Flexural Mode $i = 2$	Second Flexural Mode $i = 3$	Third Flexural Mode $i = 4$	Fourth Flexural Mode $i = 5$	Fifth Flexural Mode $i = 6$
In Air					
Computed*	365	438	574	790	1080
Experimental	365	440	580	790	1020
In Water, atmospheric pressure					
Computed**	204	250	339	480	662
Experimental	-	250	330	480	-
* $\xi = 3.35 \times 10^4$, $\eta = 626 \times 10^4$, $\zeta = 0$.					
** $\xi = 1.304 \times 10^4$, $\eta = 191 \times 10^4$, $\zeta = 0$.					

The theoretical frequency equation for the vibration of a ring with elastic support in air employed in the preceding correlation is²

$$p_i^2 = \frac{i^2(1-i^2)^2}{1+i^2} \xi + \frac{i^2}{1+i^2} \eta + \frac{1}{1+i^2} \zeta \quad [1]$$

where ξ , η , and ζ are lumped constants

$$\xi = \frac{E I g}{A \gamma r^4}$$

$$\eta = \frac{k g}{A \gamma}$$

$$\zeta = \frac{m g}{A \gamma}$$

and p_i is the resonance frequency in radians per second corresponding to an integer i ,

l is an integer designating the mode of vibration,

r is the radius of the ring in inches,

A is the cross-sectional area of the ring in inches²,

I is the moment of inertia of cross section of the ring about the $x-x$ axis in inches⁴,

k is the assumed modulus of radial elastic support in pounds per inch per inch,

m is the assumed modulus of tangential elastic support in pounds per inch per inch,

E is the modulus of elasticity in pounds per square inch,

γ is the weight density in pounds per cubic inch, and

g is the acceleration due to gravity, 386 in/sec².

The values for the lumped constants of $\xi = 3.35 \times 10^4$ and $\eta = 626 \times 10^4$ in air, and $\zeta = 1.304 \times 10^4$ and $\eta = 191 \times 10^4$ in water used for correlation are obtained by simultaneously solving the frequency equation at $i = 2$ and $i = 5$, and at $i = 3$ and $i = 5$, respectively, using the experimental frequencies obtained for these modes assuming radial support only. At the present time it is not possible to compute the lumped coefficients independently.

An additional comparison between measured and computed resonance frequencies based on Bleich's analysis can also be made. However, it should be noted that any numerical computations made with this method are tentative and may be subject to revision upon publication of the completed analysis of the problem. The calculated results for the resonance frequencies of the lobar modes for the model in air are given in Table 7 for the case where the radial motion varies sinusoidally between bulkheads, $L_b = 2R$, and for the case of three identical sections attached together having a variation in radial amplitude varying sinusoidally between the end bulkheads of the outermost sections, $L_b = 6R$. This computation indicates that the higher modes, $i = 4$ and $i = 5$, are associated with the $L_b = 2R$ configuration while the lower frequencies correspond more closely to the $L_b = 6R$ configuration. Although the model tested

TABLE 7

Comparison of Experimental Frequencies of Lobar Vibration of Model DR201 in Air with Those Computed by Bleich Theory

	Frequency, cps				
	First Flexural Mode <i>i</i> = 2	Second Flexural Mode <i>i</i> = 3	Third Flexural Mode <i>i</i> = 4	Fourth Flexural Mode <i>i</i> = 5	Fifth Flexural Mode <i>i</i> = 6
Experimental	365	440	580	790	1020
Bleich, $L_b = 2R$	788	508	<u>547*</u>	<u>755</u>	<u>1240</u>
Bleich, $L_b = 6R$	<u>197</u>	<u>391</u>	652	927	1412

*The underlined computed values give closest agreement with the experimental values.

comprises only one section, $L_b = 2R$, the above correlation might be possible if the radial motion for the experimental $i = 2$ and $i = 3$ modes were not zero at the bulkheads. A more complete comparison could be made by testing a model comprising three sections attached together. The underlined computed values in Table 7 based on the above observations give closest agreement with experiment. From this correlation it would appear that the Bleich theory is of value in roughly estimating the resonance frequencies of lobar vibration of a stiffened cylindrical shell of the given model geometry. It is expected that the $i = 2$ comparison might have been better if the closed end bulkhead and serrated mounting flange, not taken into account in the computation, had not been attached to the model. In this connection, part of the current research on this problem at the Taylor Model Basin includes the determination of the resonance frequencies of lobar vibration of various models being constructed for research on the static strength of submarines, before and after test ends are attached. It is intended that these experimental results will serve to evaluate better the utility of the above theory.

Owing to virtual-mass effects of water surrounding the model, the observed resonance frequencies in water are only approximately 60 percent as large as the previously discussed experimental resonance frequencies in air. A slight variation in this percentage, from about 57 percent at $i = 3$ to 61 percent at $i = 5$, is noted for the various modes.

If the theoretical virtual mass Δm is considered to be the amount by which the effective mass of the model is increased in water, then the relationship between the frequencies in air and in water is

$$p_{iw}^2 = p_{iA}^2 \left(\frac{1}{1 + \frac{\Delta m}{m_s}} \right) \quad [2]$$

where

$$\Delta m = r \gamma_w \frac{i}{i^2 + 1} \quad (\text{see Reference 11}) \quad [2a]$$

$$m_s = \gamma_s \lambda \quad [2b]$$

and p_{iA} is the natural circular frequency in air,

p_{iw} is the natural circular frequency in water,

i is an integer designating the mode of lobar vibration,

γ_s is the volume density of steel,

γ_w is the volume density of water,

r is the radius of the cylinder, and

λ is the thickness of the shell.

The ratio $\Delta m/m_s$ can be considered equivalent to twice the ratio of the mass of the volume of water displaced by a unit length of shell to the mass of the shell involved multiplied by a mode shape factor $i/(i^2 + 1)$ and in this case is equivalent to $11.05 i/(i^2 + 1)$. Evaluating the ratio of the frequency in water to the frequency in air,

$$K_i = \sqrt{\frac{1}{1 + \frac{\Delta m}{m_s}}}$$

gives the following values for K_i for the various mode shapes:

i	K_i
2	0.425
3	0.475
4	0.527
5	0.566
6	0.599

This indicates that the frequencies in water are 42.5 percent as large as the frequencies in air at $i = 2$ and 56.6 percent at $i = 5$. In comparison with experimental values, the theoretical virtual-mass correction lowers the frequency 10 percent more than that observed at $i = 3$ and 4 percent lower than observed at $i = 5$. Both experiment and theory indicate that the effect of virtual mass is greater at the higher modes than at the lower modes. The discrepancy observed between theory and experiment may possibly be attributed to the fact that the model was not suspended in an infinite fluid medium.

In addition to effects of virtual mass of surrounding water on the resonance frequencies, it is noted from the experimental results, Figure 12, that an increase in hydrostatic pressure causes a further decrease in the resonance frequencies. It has been shown by Kennard that the analogous frequency equation for an elastically supported ring in air, taking into account the presence of uniform pressure on outside surface, becomes:

$$p_i^2 = \frac{i^2}{1+i^2} \frac{g}{Ay} \left[\frac{El}{r^4} (i^2-1)^2 + k + \frac{m}{i^2} - \frac{P_0}{r} (i^2-1) \right] \quad [3]$$

where $P_0 = \delta P$ (lb/in. of circumference) or hydrostatic pressure times ring width. If the theoretical correction for virtual mass of surrounding water given in the preceding discussion is applied to this equation, the frequency equation for the elastically supported ring surrounded by water around the outer periphery and including the effects of external hydrostatic pressure becomes, for $m = 0$ (no tangential support):

$$p_{i_w}^2 = \frac{i^2}{1+i^2 + \frac{r\rho_w i}{\gamma h}} \left[\xi(i^2-1)^2 + \eta - \frac{Pby}{Ay r} (i^2-1) \right] \quad [4]$$

Substituting in the above the values of $\xi = 8.35 \times 10^4$ and $\eta = 626 \times 10^4$ in air, determined previously, and assuming the hydrostatic loading effective over one frame space, the dotted curves paralleling the experimental curves in Figure 12 are obtained.* The correlation shown between theory and experiment for the effect of hydrostatic pressure on the resonance frequencies is excellent. The frequencies computed above are lower than those observed because of the previously mentioned difference between theoretical and experimental virtual-mass effects.

CONCLUSIONS

From the results presented, the following observations and deductions can be drawn:

1. The occurrence of an initial shell bulge in Model DR201 at 425 psi well in advance of final collapse pressure (495 psi) is attributed to the presence of lobar vibration during hydrostatic test.
2. The observed difference between final collapse pressures for Models DR201 and DR202 (495- 515 psi) while small is due to lobar vibration of Model DR201. If both models had been constructed of shell material having the same yield strength, Model DR202 would have failed at a higher hydrostatic pressure and the difference would have been more marked.
3. The failure (shell yield) at a lower pressure for the vibrated model can be explained by superposition of dynamic stresses upon hydrostatic stresses such that the sum equals the yield of the material based on uniaxial strain measurements.
4. The frequencies of vibration in air may be computed empirically from the equations of an elastically supported ring and may be approximately determined for the higher modes by the analytic method of Bleich.

*It is noted here from Equation [4] that the effect of the hydrostatic pressure on the frequency would be more evident if Elg/Ayr^4 or ξ were smaller; this would be the case if the stiffening rings were smaller, i.e., if failure would occur by general instability.

5. Due to virtual-mass effects of water surrounding the model, the observed resonance frequencies in water are only approximately 60 percent as large as the frequencies in air. The theoretical reduction in resonance frequencies can be computed from virtual-mass effects in water, Equation [2], and varies from 42.5 percent at $i = 2$ to 59.9 percent at $i = 6$.

6. The observed frequencies of lobar vibration decrease with an increase of hydrostatic pressure. The amount by which these frequencies are lowered due to hydrostatic pressure may be obtained from Equation [4], which incorporates the theoretical effects of virtual mass and hydrostatic pressure into the frequency equation of an elastically supported ring.

7. Under combined loading, the amplitude of vibration of the model for a constant driving force increased as hydrostatic pressure was applied up to 250 psi but above this, pressure decreased and followed a cyclic path. From comparison with elementary theory it was shown that the amplitude should have steadily increased as the pressure was applied. The observed behavior was attributed to a coupling action between the model and the pressure tank. Future tests of this nature should be made with a model completely free from the tank itself and of small diameter compared with the tank, such as a 27-in.-diameter model freely supported in the recently constructed TMB 8-ft-diameter tank.

APPENDIX

The circularity charts for Model DR201, Figures 18 through 30, show the initial circularity plotted as solid lines and the final circularity after collapse as dotted lines on polar coordinates. Readings were taken every 10 deg around the circumference except at damaged locations where they were taken at 5-deg intervals. Stations for readings were selected at each frame and bulkhead location and midway between these locations.

Figures 18-30 - Transverse Contours for Model DR201 Showing Initial Circularity and Final Deflections after Collapse

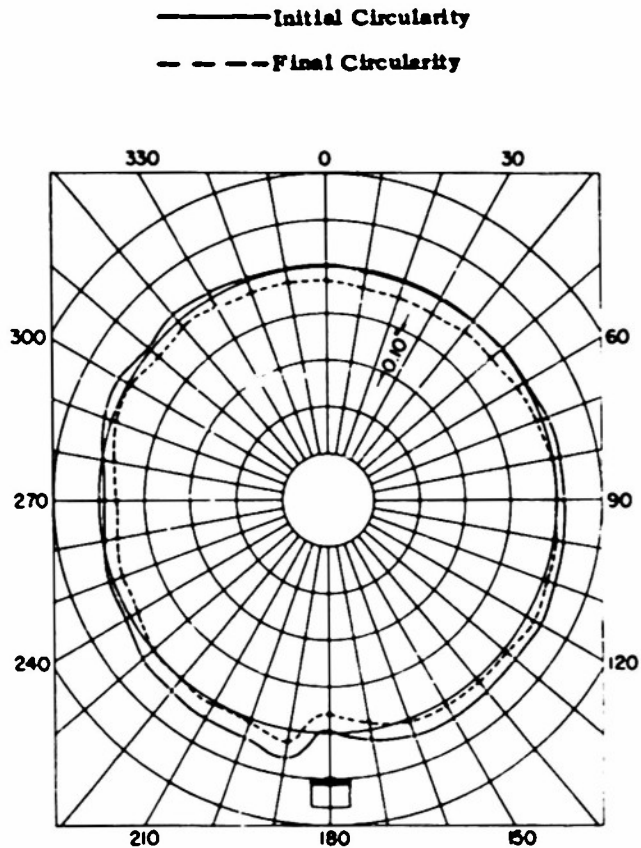


Figure 18 - Station 1, Bulkhead 1

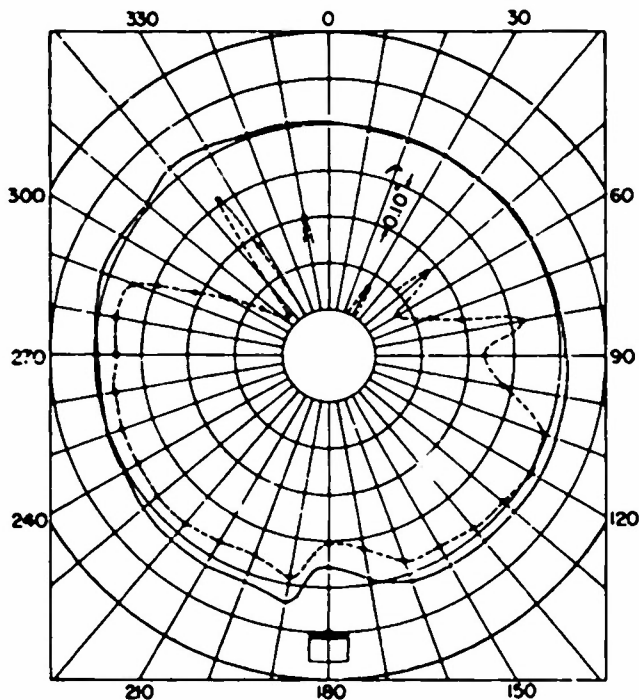


Figure 19 - Station 2, Between Bulkhead 1 and Frame 1

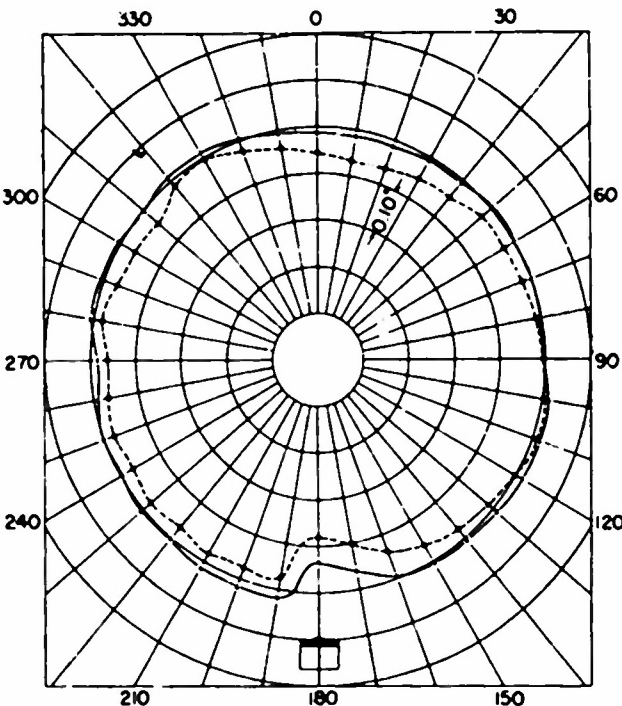


Figure 20 - Station 3, Frame 1

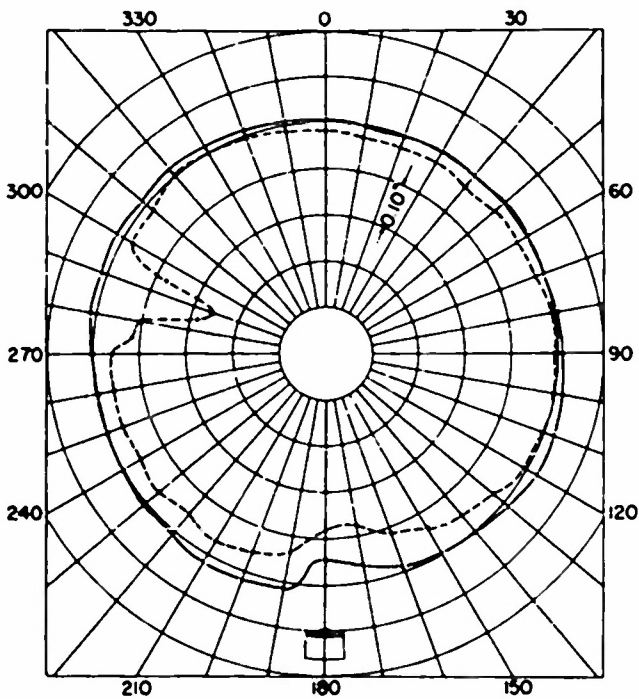


Figure 21 - Station 4, Between Frame 1 and Frame 2

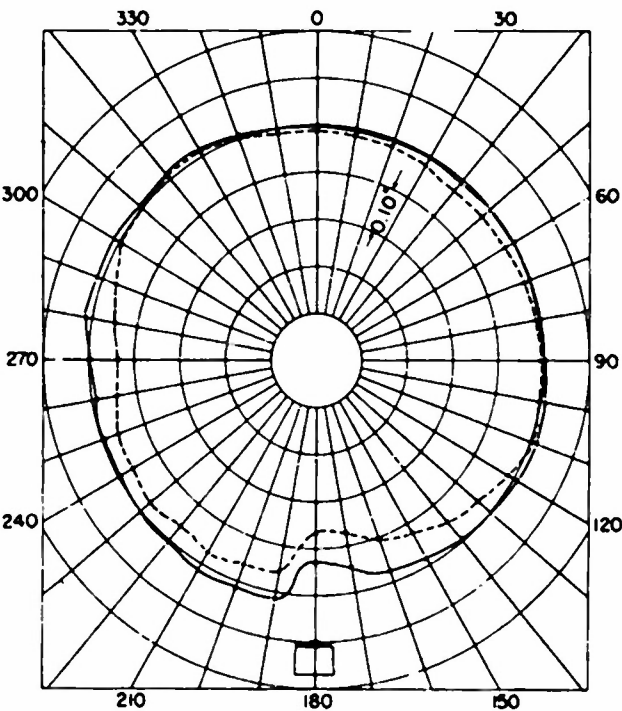


Figure 22 - Station 5, Frame 2

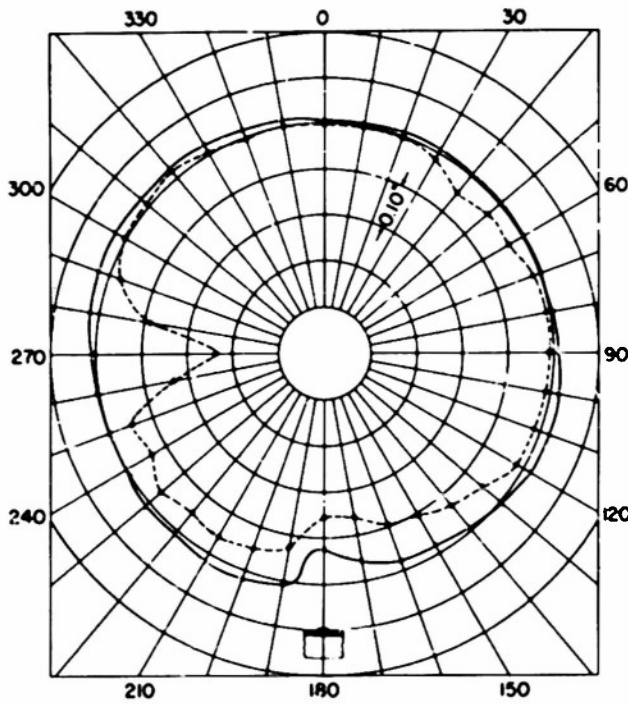


Figure 23 - Station 6, Between Frame 2 and Frame 8

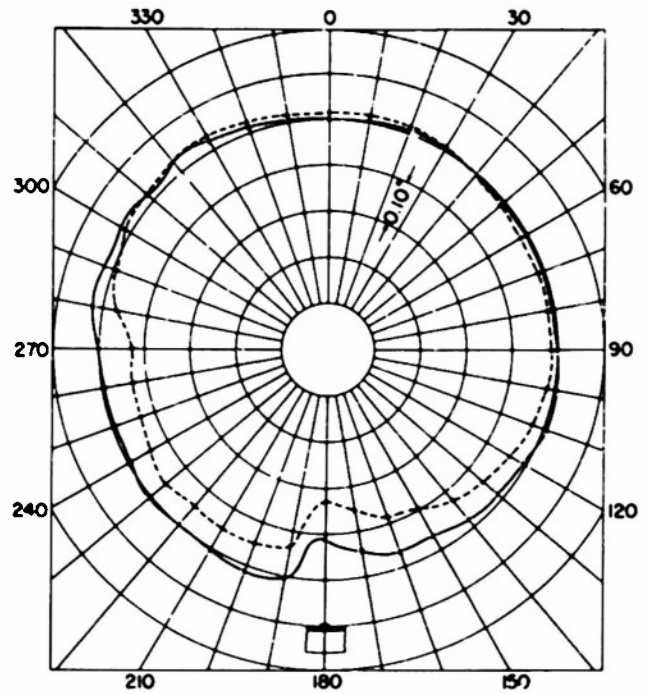


Figure 24 - Station 7, Frame 3

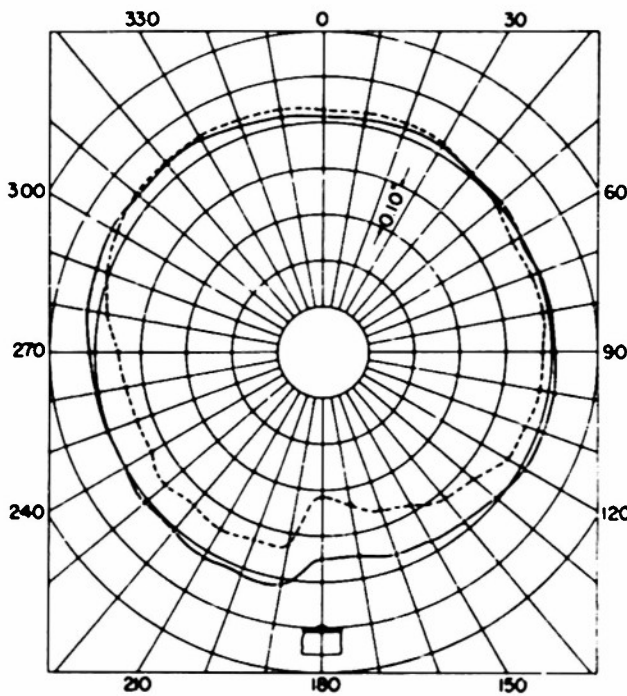


Figure 25 - Station 8, Between Frame 3 and Frame 4

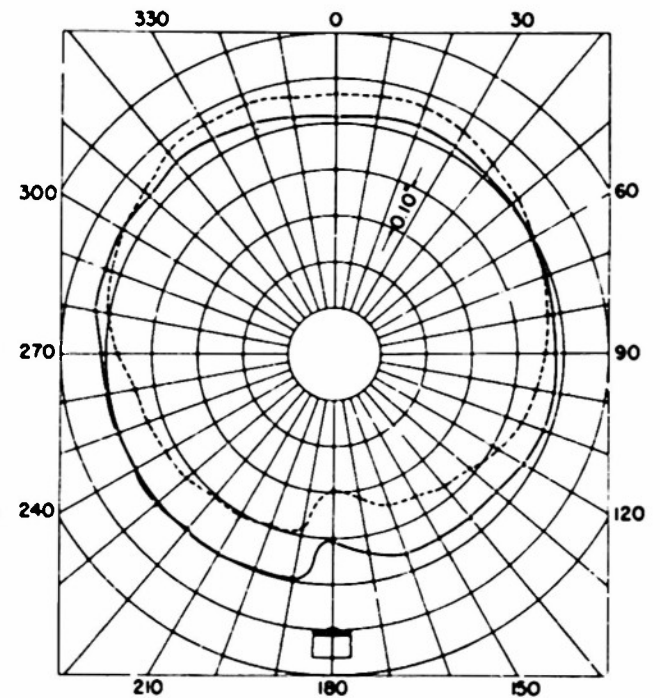


Figure 26 - Station 9, Frame 4

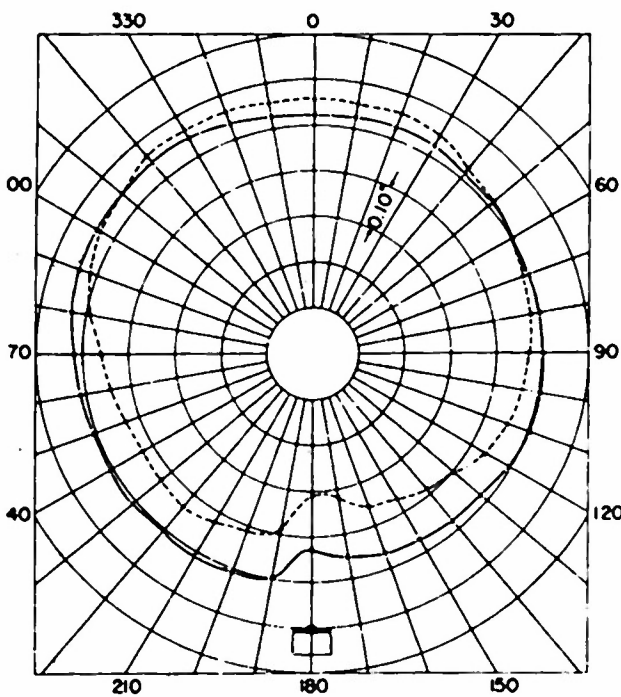


Figure 27 - Station 10, Between Frame 4 and Frame 5

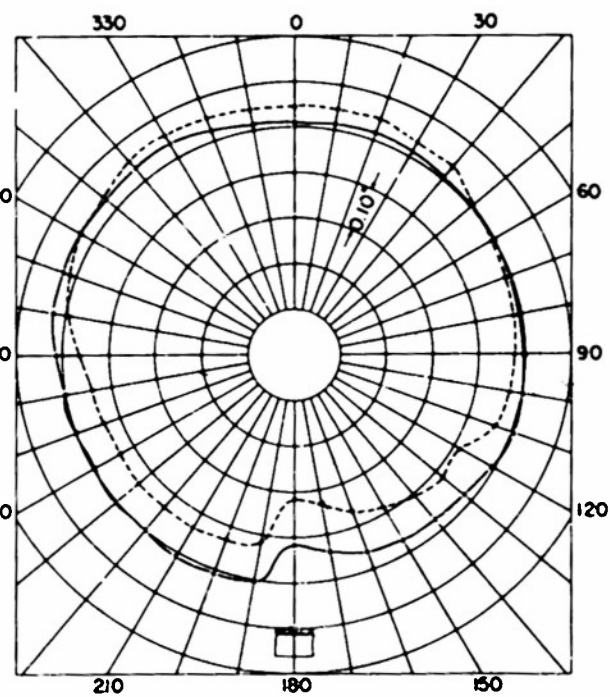


Figure 28 - Station 11, Frame 5

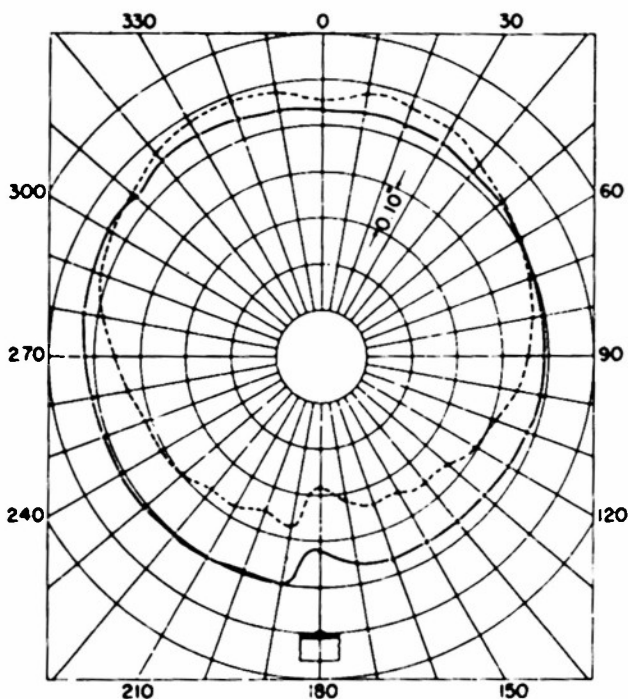


Figure 29 - Station 12, Between Frame 5 and Bulkhead 2

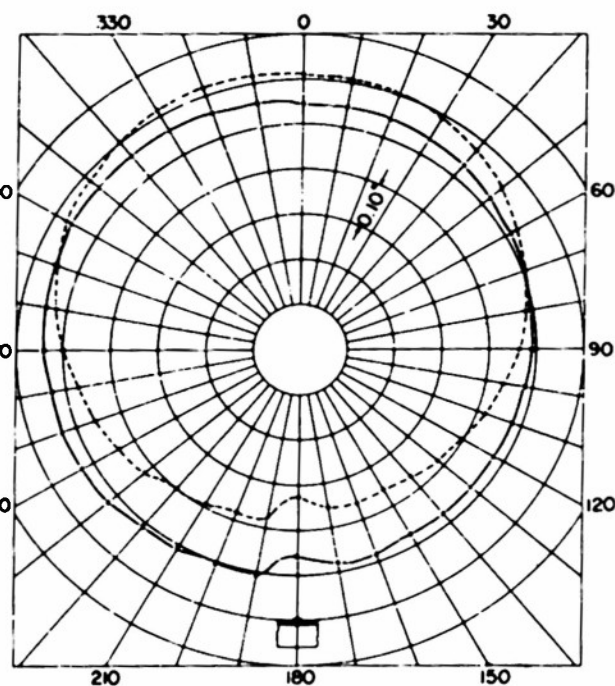


Figure 30 - Station 18, Bulkhead 2

REFERENCES

1. Research and Development Project Card, "Investigation of Submarine Structures," NS 781-088, 30 April 1951.
2. Wenk, Edward, Jr., "A Theoretical and Experimental Investigation of a Dynamically Loaded Ring with Radial Elastic Support," TMB Report 704, July 1950.
3. Wenk, Edward, Jr. and Allnut, Ralph B., "Lobar Vibrations of 1/8-Scale Models of the SS568 Pressure Hull," TMB CONFIDENTIAL Report C-354, November 1950.
4. Allnut, Ralph B. and Wenk, Edward, Jr., "Response of Stiffened Cylindrical Shells to Combined Hydrostatic Loading and Steady-State Lobar Vibrations - Part II, Tests of Models DR 203 and DR 204 Designed to Fail by General Instability," TMB CONFIDENTIAL Report C-446, in preparation.
5. Burns, Charles I., "The Residual Hydrostatic Strength of Explosively Damaged Stiffened Cylindrical Shells," TMB CONFIDENTIAL Report C-406, May 1952.
6. von Sanden, K. and Gunther, K., "The Strength of Cylindrical Shells, Stiffened by Frames and Bulkheads, under Uniform Pressure on All Sides," TMB Translation 88, March 1952.
7. Murphy, Glenn, "Advanced Mechanics of Materials," McGraw-Hill, New York, 1946.
8. Salerno, V.L. and Levine, B., "General Instability of Reinforced Shells under Hydrostatic Pressure," PIBAL Report 189, September 1951.
9. Windenburg, Dwight F. and Trilling, Charles, "Collapse by Instability of Thin Cylindrical Shells under External Pressure," TMB Report 885, July 1934.
10. Bleich, H.H., "The Source of the Dynamic Strength of Submarine Hulls," Presented at Undex Symposium, 1951, CONFIDENTIAL.
11. Bleich, H.H., "The Effect of Submergence on the Vibrations of Submarine Hulls," Presented at Undex Symposium, 1951, CONFIDENTIAL.
12. Junger, Miguel C., "Vibrations of Elastic Shells in a Fluid Medium and the Associated Radiation of Sound," Paper No. APM-28, Presented at the National Conference of Applied Mechanics Division of the ASME, June 19-21, 1952.

INITIAL DISTRIBUTION**Serials**

- 1 - 16 Chief, Bureau of Ships, Technical Library (Code 327), for distribution:
- 1 - 5 Technical Library
 - 6 Technical Assistant to Chief of Bureau (Code 106)
 - 7 Preliminary Design and Ship Protection (Code 420)
 - 8 Preliminary Design (Code 421)
 - 9 - 11 Underwater Explosion Research (Code 423)
 - 12 Hull Design (Code 440)
 - 13 - 14 Scientific, Structural and Hydromechanics (Code 442)
 - 15 - 16 Submarines (Code 515)
- 17 Chief of Naval Operations, Op 34H8
- 18 - 25 Chief of Naval Research, Mechanics and Materials Branch for forwarding to cognizant contractors
- 26 - 27 Commander, U.S. Naval Ordnance Laboratory, White Oak, Silver Spring 19, Md.
- 28 Director, Naval Research Laboratory, Anacostia 20, D.C.
- 29 - 30 Commander, Norfolk Naval Shipyard, Underwater Explosion Research Division, Code 290, Portsmouth, Va.
- 31 - 32 Commander, Portsmouth Naval Shipyard, Portsmouth, N.H.
- 33 - 34 Commander, Naval Ordnance Test Station, Inyokern, China Lake, Calif.
- 35 Commanding Officer, U.S. Naval Underwater Ordnance Station, Newport, R.I.
- 36 - 37 Commander, Mare Island Naval Shipyard, Vallejo, Calif.
- 38 - 40 Supervisor of Shipbuilding and Naval Inspector of Ordnance, General Dynamics Division, Electric Boat Co., Groton, Conn.
- 41 Director, Naval Engineering Experiment Station, Annapolis, Md.
- 42 Armed Forces Special Weapons Project, P.O. Box 2610, Washington, D.C.
- 43 Commanding General, Air Materiel Command, Wright-Patterson Air Force Base, Dayton, Ohio
- 44 Director, Langley Aeronautical Laboratory, Langley Air Force Base, Va.
- 45 - 53 British Joint Services Mission, P.O. Box 165, Benjamin Franklin Station, Washington, D.C.